Neurobiology of Disease

# Pain Hypersensitivity in SLURP1 and SLURP2 Knock-out Mouse Models of Hereditary Palmoplantar Keratoderma

**Rachel L. Weinberg,[1*] Suyeon Kim,[1,2*] Zixuan Pang,[1,2] Sandy Awad,[1] Tyger Hanback,[1,3] Baohan Pan,[4] Leonie Bettin,[1] Dennis Chang,[1,5] Michael J. Polydefkis,[4] Lintao Qu,[1] and Michael J. Caterina[1,2,5]**

[1]Department of Neurosurgery, Neurosurgery Pain Research Institute, Johns Hopkins School of Medicine, Baltimore, Maryland 21205, [2]Department of Biological Chemistry, Johns Hopkins School of Medicine, Baltimore, Maryland 21205, [3]Department of Biochemistry and Molecular Biology, Johns Hopkins School of Public Health, Baltimore, Maryland 21205, [4]Department of Neurology, Johns Hopkins School of Medicine, Baltimore, Maryland 21205, and [5]Department of Neuroscience, Johns Hopkins School of Medicine, Baltimore, Maryland 21205

**SLURP1 and SLURP2 are both small secreted members of the Ly6/u-PAR family of proteins and are highly expressed in keratinocytes. Loss-of-function mutations in SLURP1 lead to a rare autosomal recessive palmoplantar keratoderma (PPK), Mal de Meleda (MdM), which is characterized by diffuse, yellowish palmoplantar hyperkeratosis. Some individuals with MdM experience pain in conjunction with the hyperkeratosis that has been attributed to fissures or microbial superinfection within the affected skin. By comparison, other hereditary PPKs such as pachyonychia congenita and Olmsted syndrome show prevalent pain in PPK lesions. Two mouse models of MdM, Slurp1 knock-out and Slurp2X knock-out, exhibit robust PPK in all four paws. However, whether the sensory experience of these animals includes augmented pain sensitivity remains unexplored. In this study, we demonstrate that both models exhibit hypersensitivity to mechanical and thermal stimuli as well as spontaneous pain behaviors in males and females. Anatomical analysis revealed slightly reduced glabrous skin epidermal innervation and substantial alterations in palmoplantar skin immune composition in Slurp2X knock-out mice. Primary sensory neurons innervating hindpaw glabrous skin from Slurp2X knock-out mice exhibit increased incidence of spontaneous activity and mechanical hypersensitivity both in vitro and in vivo. Thus, Slurp knock-out mice exhibit polymodal PPK-associated pain that is associated with both immune alterations and neuronal hyperexcitability and might therefore be useful for the identification of therapeutic targets to treat PPK-associated pain.**

*Key words:* **hyperalgesia; Mal de Meleda; pain; palmoplantar keratoderma; SLURP**

**Significance Statement**

**Palmoplantar keratodermas (PPKs) are rare human skin disorders associated with thickening of the skin on the palms and soles. Pain is a common feature of some PPKs, yet the causes of PPK-associated pain are not understood. Here we show that two mouse models of one PPK, knock-out mice lacking either SLURP1 or SLURP2, secreted modulators of nicotinic acetylcholine receptors, exhibit enhanced pain sensitivity and increased activity of pain-associated sensory neurons. These mouse lines will therefore be of value in defining causes of pain in PPKs and possibly developing improved therapies for that pain.**

## Introduction

Hereditary palmoplantar keratodermas (PPKs) are a group of rare skin disorders, caused by mutations in any of at least 25 different genes, that are characterized by abnormal thickening of the plantar skin of the hands and feet. Hereditary PPKs vary with respect to anatomical pattern (i.e., focal, punctate, or diffuse), lesion histology, and involvement of secondary structures, but all exhibit expansion of the viable epidermis (Schiller

Received Feb. 11, 2023; revised April 30, 2024; accepted May 22, 2024.

Author contributions: R.L.W., S.K., Z.P., B.P., M.J.P., L.Q., and M.J.C. designed research; R.L.W., S.K., Z.P., S.A., T.H., B.P., L.B., D.C., and L.Q. performed research; R.L.W., S.K., Z.P., S.A., T.H., B.P., L.B., D.C., M.J.P., L.Q., and M.J.C. analyzed data; R.L.W., S.K., L.Q., and M.J.C. wrote the paper.

This work was supported by the Neurosurgery Pain Research Institute at Johns Hopkins School of Medicine (M.J.C., L.Q.) and the Boehringer Ingelheim Veterinary Scholars Program (L.B.). We thank Dr. Stephen Young (UCLA) for providing the Slurp1 KO mice and Slurp2X KO breeder mice. We also thank Dan Bennett, Neil Bolduc, Ian Reucroft, and John Robinson for mouse colony maintenance, Xiaobu Ye for statistical consultation, and Pierre Coulombe and members of the Caterina, Qu, and Alexandre/Latremoliere labs for helpful suggestions. This article was prepared while Dr. Rachel Weinberg was employed at Johns Hopkins. The opinions expressed in this article are the author's own and do not reflect the view of the National Institutes of Health, the Department of Health and Human Services, or the United States government.

*R.L.W. and S.K. contributed equally to this work.

The authors declare no competing financial interests.

Correspondence should be addressed to Michael J. Caterina at caterina@jhmi.edu or Lintao Qu at qulintao76@yahoo.com.

L.Q.'s present address: Hengyang Medical School, Clinical Research Institute, The Second Affiliated Hospital of University of South China, Hengyang, Hunan 41001, China.

https://doi.org/10.1523/JNEUROSCI.0260-23.2024

Copyright © 2024 the authors

et al., 2014; Has and Technau-Hafsi, 2016; Sakiyama and Kubo, 2016). Some individuals with hereditary PPK also experience chronic pain or itch, varying in prevalence among specific PPKs, that can severely impact quality of life. Yet, the rarity of hereditary PPKs has impeded understanding the mechanisms behind this pain. As a consequence, treatment of PPK-associated pain remains suboptimal.

Mal de Meleda (MdM) is an autosomal recessive diffuse hereditary PPK first characterized in 1826 on the Croatian island of Mljet. Symptoms associated with MdM include diffuse, yellowish palmoplantar hyperkeratosis, nail anomalies, perioral erythema, odor, and increased risk of malignant melanoma (Perez and Khachemoune, 2016). MdM is caused by a mutation in the gene encoding secreted lymphocyte antigen 6/urokinase-type plasminogen activator receptor related protein-1 (SLURP1). SLURP1 is a secreted protein of the Ly6/u-Par family and is proposed to bind to α7 nicotinic acetylcholine receptors on keratinocytes to stimulate proapoptotic activity and late-stage differentiation (Chimienti et al., 2003; Arredondo et al., 2005; Favre et al., 2007). SLURP1 has also been shown to regulate T-cell activity and TNF-α suppression (Chimienti et al., 2003; Saftić et al., 2006; Tjiu et al., 2011). In a recent study, immunohistochemical analysis of MdM revealed prolific TNF-α expression within the epidermis and dermal perivascular infiltrates indicating a heightened inflammatory environment (Kudo et al., 2020). Individuals with MdM sometimes report pain, but not with the prevalence seen in certain other PPKs. In studies that mention this symptom, it has been attributed to the thickness or lesions of the skin or to secondary microbial infections (Charfeddine et al., 2006; Wajid et al., 2009; Morais e Silva et al., 2011; Kalyan et al., 2021). Therapies used in MdM have included moisturizers, antifungal creams, oral acitretin, or vitamin A tablets, though these tend to be ineffective (Morais e Silva et al., 2011; Kalyan et al., 2021).

Mouse models of MdM harboring loss-of-function mutations in either SLURP1 or a closely related gene, SLURP2, also display epidermal thickening of plantar skin, on both front and hindpaws, beginning at ∼6 weeks of age (Adeyo et al., 2014; Allan et al., 2016). Knock-out of either gene also results in alterations in body size and lipid metabolism, as well as a paw clasping phenotype of unknown pathophysiology. Double knock-out of SLURP1 and SLURP2 produced a similar phenotype with no apparent additivity (Allan et al., 2018). Here we set out to determine if SLURP1 and SLURP2 knock-out mouse models of MdM could be used to assess PPK-associated pain to explore potential mechanisms that might lead to more targeted treatments for individuals with these disorders.

## Materials and Methods

*Mice.* Slurp1$^{-/-}$ (Slurp1 KO) mice and Slurp2X$^{-/-}$ (Slurp2X KO) mice, previously described (Adeyo et al., 2014; Allan et al., 2016), were generously provided by Dr. Stephen Young (UCLA). Wild-type and homozygous null mice used for experiments were generated by mating heterozygotes and were sex matched and age matched within 1–2 weeks but were not always littermates. Both male and female mice were examined. Mice used for experiments were greater than 6 weeks old. Slurp1 KO mice were on a C57Bl/6J background. Slurp2X KO mice used in our initial experiments were on a mixed SVE-129 and C57Bl/6J background but were later backcrossed onto a C57Bl/6J background for at least eight generations. The approximate extent of backcross is indicated in the figure legends. Animals were housed 1–5 per cage under a 14/10 h light/dark cycle with *ad libitum* access to food and water. In some cases, food was supplemented with fenbendazole to control pinworm infections in the facility. All experiments adhered to the National Institutes of Health Guide for the Care and Use of Laboratory Animals and were performed according to protocols approved by our Institutional Animal Care and Use Committee.

*Behavioral experiments.* All experiments were conducted on awake, free-moving, age-matched mice with experimenter nominally blinded to genotype. However, knock-out mice had clearly developed PPK of the front and hindpaws at the time of testing, compromising true blinding. Von Frey analysis was used to assess punctate mechanical sensitivity. Mice were acclimated in plexiglass boxes on top of a wire mesh for 2 h per day for 2 d before experimentation. A series of nylon filaments of increasing force were applied perpendicularly to the glabrous skin of the hindpaws to the point of bending. To generate force–response curves or quantify responsiveness at a given force, unless otherwise noted, each force was applied to the right and left hindpaws five times for a total of 10 measurements. The number of positive responses out of 10 trials was calculated as a percent and used for analysis. In some cases, we instead utilized the up-down method to calculate a 50% withdrawal threshold (Chaplan et al., 1994). The nominal bending forces of the filaments, provided by the manufacturer, 0.02, 0.04, 0.07, 0.16, 0.4, 0.6, 1, and 1.4 g, are shown in the figures.

A radiant paw heating assay was used to assess hindpaw thermal nociception. Animals were acclimated in a plexiglass box on a glass surface for 2 h per day for 2 d before experimentation. A noxious heat stimulus was applied to the plantar region of the hindpaw using a radiant heat source (Plantar Test Apparatus, IITC Life Science) and time to paw withdrawal was recorded. A cutoff time of 15 s was established to prevent tissue injury. Three to four repeated measurements were conducted for each paw, 10 min apart, and the average was used for analysis. A laser stimulation assay was used to assess thermal nociception in front paw plantar skin. Animals were acclimated in a plexiglass box on a glass surface for 2 h per day for 2 d before experiment. A 445 nm blue portable laser (Shanghai Laser & Optics Century, Model BLM445P8-200) with an output power of ∼200 mW was directed at the plantar surface of the front paw, and time to front paw withdrawal was recorded by a stopwatch. Three to five repeated measurements were conducted for both paws, 10 min apart, and the average over both paws was used for analysis. The tail immersion assay was used to test thermal nociception in tail skin. Mice were gently restrained in a handheld towel and their tail partially submerged in a water bath at 48°C. Three to five measurements of time to tail withdrawal were recorded 10 min apart and the average was used for analysis.

A capsaicin injection assay was used to assess chemical nociception. Animals were acclimated in plexiglass cylinders for 2 h per day for 2 d before experimentation. Vehicle (5% ethanol/0.25% Tween 80 in saline) was injected subcutaneously into the plantar surface of one hindpaw, and time spent licking the hindpaw was measured over 10 min. Forty-eight hours later, capsaicin (1 µg in 10 µl 5% ethanol/0.25% Tween 80 in saline) was injected into the opposite paw and licking measured in the same way.

To examine any nonevoked pain behaviors the mice may have been exhibiting, animals were acclimated in plexiglass chambers on a glass surface and recorded for 10 min. In order to keep the mouse awake, plexiglass chambers were moved slightly at regular intervals throughout recording. Instances of front paw guarding, front paw flinching, front paw licking, and hindpaw licking were quantified using X-PloRat analysis software (Tejada et al., 2018). Both episode numbers and duration of defined behaviors were scored by a blinded observer. Behaviors were defined as instances of front paw guarding (mouse withdraws front paw toward its body), paws on glass (mouse has both front paws flat on the glass surface), front paw flinching (mouse quickly shakes its front paw), and front paw and hindpaw licking (often associated with spreading of digits).

*Indomethacin pharmacology.* Mice were acclimated in plexiglass boxes 2 h/d for 2 d before experimentation. A baseline von Frey analysis was performed at 1 g force followed by a baseline radiant paw heating analysis as described above. Indomethacin [Millipore, 10 mg/kg in 10% 0.1 M $Na_2CO_3$ in phosphate-buffered saline (PBS), pH ∼7] or vehicle (pH adjusted with 5 M HCl) was injected intraperitoneally into mice and radiant paw heating assay was conducted beginning at 30 min (range 30–50 min) and again beginning at 2 h (range, 120–140 min) after the last mouse was injected. Von Frey analysis was conducted ∼3.5 h after

the last mouse was injected. After a wash-out period of at least 5 d, mice were injected intraperitoneally with the solution (vehicle or indomethacin) that they had not previously received, and the behavioral assays were repeated. All behavior was conducted blinded to injected agent. For spontaneous behavior recordings, mice were filmed for 10 min, 2 h post-intraperitoneal indomethacin injections on a glass surface, and behaviors were scored as described above. One week later, the mice were injected intraperitoneally with the alternate solution (vehicle or indomethacin) and the recordings repeated.

*Gabapentin pharmacology.* Mice were acclimated in plexiglass boxes 2 h/d for 2 d before experimentation. A baseline von Frey analysis was performed using the up-down method followed by a baseline radiant paw heating analysis as described above. Gabapentin (Sigma, 100 mg/kg in saline) or saline was injected intraperitoneally, and the radiant paw heating assay was conducted beginning at 30 min (range, 30–50 min) after the last mouse was injected. Von Frey analysis was conducted 2 h (range, 120–140 min) after the last mouse was injected. All behavior was conducted blinded to the agent injected.

*DRG neuron culture.* Hindpaw-innervating neurons were retrogradely labeled with 1,1′-dioctadecyl-3,3,3′,3′-tetramethylindocarbocyanine perchlorate (DiI, Sigma, 2.5 mg/ml in 25% EtOH 15 µl). One week after DiI labeling, L4/L5 dorsal root ganglia (DRGs) were harvested and washed in complete saline solution (CSS) containing the following (in mM): 137 NaCl, 5.3 KCl, 10 glucose, 10 HEPES, with pH adjusted to 7.2–7.4, and osmolarity adjusted to 290–300 mOsm with mannitol. DRGs were digested in Liberase TM (Roche Diagnostics) and 0.5 mM EDTA in CSS for 20 min, centrifuged (800 rpm, 3 min), and digested for another 15 min in Liberase TL (Roche Diagnostics) supplemented with papain (20–30 U/ml, Worthington Biochemical) and 0.5 mM EDTA in CSS. Both digestions occurred at 37°C. The tissue was then centrifuged again, resuspended in DMEM:F12 (Corning) containing trypsin inhibitor (1 mg/ml; Sigma) and BSA (1 mg/ml; Sigma), and triturated. After trituration, dissociated neurons were spotted onto glass coverslips precoated with poly-L-lysine (Sigma) and laminin (Thermo Fisher Scientific) and allowed to adhere for 45 min at 37°C before wells were flooded with medium containing DMEM:F12 (Corning), 10% heat-inactivated FBS (Hyclone), 1% GlutaMAX (Invitrogen), and 1% penicillin and streptomycin (Invitrogen). Cells were maintained in 5% $CO_2$ at 37°C in a humidified incubator overnight, and electrophysiology was performed within 16–24 h.

*Patch-clamp recordings.* DiI-labeled small-diameter (≤25 µm) DRG neurons were identified using a Nikon TE200 inverted fluorescence microscope, and whole-cell electrophysiology recordings were performed using an Axopatch 200B amplifier with pClamp 10 software (Molecular Devices; Qu et al., 2011, 2012). Signals were sampled at 10 kHz and filtered at 2 kHz. Pipettes were pulled from borosilicate glass capillaries (Sutter Instruments) using a P97 micropipette puller (Sutter Instruments) and had a resistance of 3–4 MΩ. Resting membrane potential (RMP) was recorded for each neuron in current-clamp mode after stabilization (within 3 min). Neurons were included if the RMP was more negative than −40 mV and the spike overshoot was >15 mV. Action potentials (APs) were evoked by a series of depolarizing current steps, each 350 ms duration, in increments of 50 pA delivered through the recording electrode. The number of APs evoked by a suprathreshold stimulus was estimated by injecting a 350 ms depolarizing current of a magnitude twice the rheobase. Input resistance was obtained from the slope of a steady-state current–voltage plot in response to a series of hyperpolarizing currents steps from −200 to −50 pA in increments of 50 pA. Capacitance (pF) was read directly from the meter on the amplifier. For current-clamp recordings, the internal solution contained the following (in mM): 120 $K^+$-gluconate, 20 KCl, 1 $CaCl_2$, 2 $MgCl_2$, 11 EGTA, 10 HEPES-$K^+$, 2 MgATP, with pH adjusted to 7.2 using Tris-base and osmolarity adjusted to 290–300 mOsm with sucrose. The external solution contained the following (in mM): 145 NaCl, 3 KCl, 2 $MgCl_2$, 2 $CaCl_2$, 10 glucose, and 10 HEPES, with pH adjusted to 7.4 with NaOH. The liquid junction potential of 11 mV was corrected.

*In vivo electrophysiology recordings.* The lumbar vertebral column of DiI-injected animals was exposed, and a laminectomy was performed from levels L2-S1 under isoflurane anesthesia delivered via intratracheal ventilation (SomnoSuite, Kent Scientific). The L4 DRG was exposed and submerged in oxygenated artificial cerebrospinal fluid (ACSF) within a pool formed by a ring to which the skin was sewn. ACSF contained the following(in mM): 130 NaCl, 3.5 KCl, 24 $NaHCO_3$, 1.25 $NaH_2PO_4$, 1.2 $MgCl_2$, 1.2 $CaCl_2$, and 10 dextrose, which was bubbled with 95% $O_2$ and 5% $CO_2$ and had a pH of 7.4 and an osmolality of 290–310 mOsm. After removal of the epineurium, the neurons on the surface of the DRG were viewed by reflection microscopy on a Nikon A1 upright confocal microscope (Nikon) and an infrared camera (DAGE-MTI). Epifluorescence imaging was used to identify DiI-labeled hindpaw-innervating neurons. Extracellular recordings were made on individual DRG cell bodies using a polished suction micropipette electrode with a tip of size 20–30 µm. The occurrence of APs was recorded extracellularly using a MultiClamp 700B amplifier and pClamp 10 software (Molecular Devices). The peripheral receptive field (RF) of an individual paw-innervating DRG neuron was identified by probing the skin over and around the exposed foot with a handheld blunt glass probe. Only DRG neurons that had a mechanical RF in the hindpaw glabrous skin were included, since PPK is prevalent across the plantar paw skin of Slurp knock-out mice. The mechanical sensitivity of paw sensory afferents was assessed by poking their RF with a set of calibrated von Frey monofilaments with a fixed tip diameter (100 µm, 5–40 mN). Each monofilament was applied for 2 s with an interstimulus interval of 3 min. Mechanical responses were quantified as the mean number of evoked APs during 2 s mechanical stimulation. The neuron was classified as spontaneously active only if spontaneous ongoing discharges occurred during a 3 min period without any external stimulation. Mechanically evoked afterdischarge was defined as APs observed in the 2 min immediately after removal of a mechanical stimulus from the RF. To avoid the confounds of abnormal activity, force–AP relations were analyzed only in neurons that exhibited neither SA nor mechanically evoked afterdischarges. Conduction velocity (CV) was obtained by electrically stimulating the RF with two wire electrodes and calculated by dividing the conduction distance between the stimulation electrode and the soma of the recorded neurons by the latency to a spike peak (Qu and Caterina, 2016; Wang et al., 2019).

*Immunohistochemistry.* For hematoxylin and eosin (H&E) analysis, hindpaw glabrous skin and tail skin were collected immediately after $CO_2$ asphyxiation, fixed in neutral buffered formalin (NBF), embedded in paraffin, sectioned, and stained with H&E. For immune cell analysis, hindpaw plantar skin was collected immediately after $CO_2$ asphyxiation or transcardial perfusion with PBS and 4% paraformaldehyde (PFA). Tissues were postfixed in NBF or 4% PFA overnight at 4°C, cryoprotected in 30% sucrose for at least 24 h at 4°C, embedded in Tissue-Tek optimal cutting temperature compound (OCT, Sakura), and stored at −80°C until cutting. Tissues were sectioned on a cryostat at 16 µm and thaw mounted onto slides. Immunofluorescence targets were detected with the following primary antibodies: rat anti-CD3 (1:50; BD Biosciences 555273), rat anti-CD68 (1:500; BioLegend 137001), rat anti-CD207 (1:400; Dendritics DDX0362P), or with Avidin-Texas Red (1:250, Invitrogen A820), washed, incubated with Alexa 488-conjugated donkey anti-rat (1:500; Jackson ImmunoResearch 712-545-153) or Alexa 488-conjugated goat anti-rat (1:500; Jackson ImmunoResearch 112-545-003), and washed again. Cell nuclei were counterstained with DAPI, and slides were coverslipped using Dako mounting media (Agilent S3023) or ProLong Gold (Invitrogen P36930).

For DRG staining, mice were perfused transcardially with PBS and 4% PFA the L4–L5 DRGs harvested. Tissues were postfixed in 4% PFA overnight at 4°C, cryoprotected in 30% sucrose for at least 24 h at 4°C, embedded in OCT, and stored at −80°C until cutting. Tissues were sectioned on a cryostat at 16 µm and thaw mounted onto slides. Immunofluorescence targets were detected with rabbit anti-CGRP (1:2,000; ImmunoStar 24112), goat anti-GFRα2 (1:400; R&D Systems AF429), and Biotin-IB4 (1:100; Sigma L2140). This was followed by Cy3-conjugated donkey anti-rabbit (1:500; Jackson ImmunoResearch 711-165-152), Alexa 488-conjugated donkey anti-goat (1:500; Jackson

ImmunoResearch 705-545-147), and DyLight 405 Streptavidin conjugate (1:500; Jackson ImmunoResearch 016-470-084).

For intraepidermal nerve fiber density (IENFD) counting, hindpaw footpads and glabrous skin were collected as above and fixed in Zamboni's fixative for 24 h, cryoprotected in 30% sucrose for at least 24 h at 4°C, embedded in OCT, and stored at −80°C until cutting. Tissue blocks were sectioned at 50 µm. 3,3′-Diaminobenzidine (DAB) immunostaining was performed with rabbit anti-PGP 9.5 (1:10,000; Abcam AB108986) and rabbit anti-CGRP (1:10,000, ImmunoStar 24112) on free-floating sections. This was followed by Biotinylated goat anti-rabbit (VectorLabs BA1000), Avidin-Biotin Complex-HRP (VectorLabs PK6100), and DAB substrate staining (VectorLabs SK4100). Cell nuclei were counterstained with methyl green (VectorLabs H-3402-500), attached to slides, and coverslipped using DPX mountant. Fluorescent immunostaining was performed with rabbit anti-CGRP (1:400, ImmunoStar 24112) or goat anti-GFRα2 (1:400; R&D Systems AF429), on free-floating sections. This was followed by Cy3-conjugated donkey anti-rabbit (1:500; Jackson ImmunoResearch 711-165-152) and Alexa 488-conjugated donkey anti-goat (1:500; Jackson ImmunoResearch 705-545-147). Cell nuclei were counterstained with DAPI, attached to slides, and coverslipped using ProLong Gold (Invitrogen P36930).

Hindpaw macroscopic images were taken with a digital camera. H&E-stained tissues were imaged on a NanoZoomer XR slide scanner (Hamamatsu) and visualized in NDPView (Hamamatsu) or captured on an Olympus BX51 microscope. DAB images were acquired and analyzed on a Leica DM750 microscope. Fluorescent images were acquired on a Nikon Eclipse TE200 inverted epifluorescence microscope or a Nikon A1 confocal microscope and analyzed using NIS Elements software (Nikon). For immune cell analysis, 2–4 images of hindpaw glabrous skin were analyzed per animal, and immune cells were counted per unit area or expressed as percent of area above immunofluorescence threshold. For IENFD analysis, the dermal–epidermal boundary was defined based on methyl green or DAPI staining of keratinocyte nuclei, and stained intraepidermal nerve fibers were defined as those crossing the dermal–epidermal borderline using published criteria (Lauria et al., 2005). Four images of hindpaw pad skin and three images of hindpaw glabrous skin were analyzed per animal. Fiji software (Schindelin et al., 2012) was used to adjust the brightness and contrast of images for figure generation and image analysis. All parameters for image acquisition were kept consistent across all animals for a given marker with experimenter nominally blinded to genotype, though again, abnormal tissue architecture in PPK skin precluded true blinding.

*Reverse transcription polymerase chain reaction.* DRGs and paw skin were freshly harvested from wild-type mice and the total RNA was isolated using RNeasy Lipid Tissue Mini Kit (Qiagen) and subjected to reverse transcription using the RT$^2$ First Strand Kit (Qiagen). The resulting cDNAs were subjected to PCR using the following primers: for Slurp1, 5′-GCTCCTGAGCACTGAAGAAT-3′ and 5′-CTGCTCAC AGGTATAGCATCG-3′ (expected size 108 bp); for Slurp2: 5′-CTGC AATGCCACCTGTGCAAG-3′ and 5′-GTCCCTGTTGCAGAGATT GGAC-3′ (expected size, 225 bp); for GAPDH, 5′-TCAACAGCAACT CCCACTCTTCCA-3′ and 5′-ACCCTGTTGCTGTAGCCGTATTCA-3′ (expected size, 115 bp). Amplification products were visualized on ethidium bromide agarose gels.

*Experimental design and statistical analysis.* For quantification of epidermal thickness, H&E staining data passed normality tests and an unpaired two-tailed Student's *t* test with Welch's correction was used to compare genotypes. For von Frey and capsaicin behavioral measurements, repeate-measures, two-way ANOVA was used to analyze the effect of genotype at a given force. ANOVA tests were followed by post hoc Bonferroni's multiple-comparisons corrections for multiple forces. For von Frey analysis using the up-down method, a test for normality was performed and at least one genotype failed to pass normality using the Kolmogorov–Smirnov test. In order to keep statistical analysis consistent across all genotypes, a Mann–Whitney nonparametric test was used to analyze the effect of genotype. For radiant heat and laser behaviors, a test for normality was performed and at least one genotype failed to pass normality using the Kolmogorov–Smirnov test. In order to keep statistical analysis consistent across all genotypes a Mann–Whitney nonparametric test was used to analyze the effect of genotype. Tail immersion data passed normality tests, and an unpaired two-tailed Student's *t* test with Welch's correction was used to compare genotypes. In indomethacin and gabapentin experiments, mechanical and thermal sensitivity were initially analyzed through three-way ANOVA to see the overall interaction between genotype, treatment, and time. To further compare different experimental groups, two-way ANOVA with Tukey's multiple-comparisons correction was conducted. For spontaneous behavior analyses of nontreated animals, Mann–Whitney nonparametric tests were used to analyze the effect of genotype on a specific behavior. For spontaneous behavior analysis of indomethacin-treated animals, a two-way ANOVA with post hoc Bonferroni's correction was used. Multiple comparisons were accounted for using the false discovery rate (FDR) approach with the Benjamini, Krieger, and Yekutieli method and a desired *Q* of 5%. For immune cell immunostaining, an unpaired two-tailed Student's *t* test with Welch's correction was used for analysis since data passed normality tests. No corrections were made for multiple comparisons in immune cell quantifications, since distinct groups of mice were used for some of the experiments. IENFD-DAB passed normality and an unpaired two-tailed Student's *t* test with Welch's correction was used to compare genotypes. For immunofluorescent staining on DRGs and IENFD, at least one genotype failed to pass normality using the Kolmogorov–Smirnov test; hence the Mann–Whitney nonparametric test was used to compare genotypes. For electrophysiology experiments, the incidence of spontaneous activity was compared between groups using chi-squared tests. In vitro rheobase, RMP, input resistance, 2× rheobase, and capacitance were analyzed using unpaired Student's *t* test. In vivo mechanical sensitivity was analyzed using two-way ANOVA with Bonferroni's post hoc correction. All data were presented as mean ± SEM, and the criterion for statistical significance was $p < 0.05$. The exact statistical analyses for each figure can be found in the figure legends and Table 1. Sample sizes were chosen based on our pilot experiments and field conventions to accurately detect statistical significance and considering ethical animal use, experiment design, and animal availability. In most instances, the "*n*" used for analysis was the number of mice. For electrophysiology experiments, the "*n*" represented in the figure was the number of neurons. All analyses were performed using GraphPad Prism 9 and Excel.

## Results

### Slurp1 KO and Slurp2X KO mice display PPK and neuroanatomical alterations in the skin

In order to assay for potential sensory phenotypes associated with PPK, we acquired two genetic mouse models of MdM which displayed PPK in all plantar skin territories of the front and hindpaws. Slurp2X KO mice harbor a nonsense mutation in the second exon of the SLURP2 gene and display a diffuse PPK on plantar paw skin (Allan et al., 2016). While the histology mirrors that of MdM, the mutations in human patients have been found in the homologous gene, SLURP1. For this reason, we also analyzed the sensory phenotype of Slurp1 KO mice, in which the second exon is replaced by neo and lacZ cassettes (Adeyo et al., 2014). As previously described, H&E staining revealed obvious thickening of the epidermis in the pad skin and glabrous skin of the hindpaws of both knock-out lines as compared with wild-type controls (Fig. 1*A*). This was verified quantitatively for glabrous skin (Fig. 1*A*). In contrast, tail skin, in which no macroscopic signs of keratoderma were evident, exhibited no differences in epidermal thickness between wild-type and Slurp2X KO mice (Fig. 1*B*). These data confirm the presence of PPK in the Slurp1 KO and Slurp2X KO mouse models, making them suitable for sensory phenotype analysis.

A previous study reported expression of Slurp1 in rat primary sensory neurons (Moriwaki et al., 2009). We therefore examined whether either Slurp1 or Slurp2 is expressed in mouse sensory

**Table 1. Statistical analyses used in this study**

| Figure | Pre hoc | Post hoc | *N*, number of samples/animals per group |
|---|---|---|---|
| *1A* | Unpaired two-tailed Student's *t* test with Welch's correction<br>Slurp2X $t_{(22.75)} = 184.1$, $p < 0.0001$<br>Slurp1 $t_{(18.34)} = 143.6$, $p < 0.0001$ | | Slurp2X WT: 6, Slurp2X KO: 6<br>Slurp1 WT: 10, Slurp1 KO: 10 |
| *1B* | Unpaired two-tailed Student's *t* test with Welch's correction<br>Slurp2X $t_{(1.399)} = -1.848$, $p = 0.2018$ | | Slurp2X WT: 6, Slurp2X KO: 6 |
| *2A* | Two-way ANOVA:<br>Force × genotype: $F_{(6,300)} = 22.16$, $p < 0.0001$<br>Force: $F_{(4.416,223)} = 166.2$, $p < 0.0001$<br>Genotype: $F_{(1,50)} = 64.66$, $p < 0.0001$ | Bonferroni's multiple-comparisons test:<br>0.02 g: $p = 0.1098$<br>0.04 g: $p = 0.0166$<br>0.07 g: $p = 0.6903$<br>0.16 g: $p < 0.0001$<br>0.4 g: $p < 0.0001$<br>0.6 g: $p < 0.0001$<br>1.0 g: $p < 0.0001$ | Slurp2X WT: 26, Slurp2X KO: 26 |
| *2B* top | Two-way ANOVA:<br>Force × genotype: $F_{(6,60)} = 0.5458$, $p = 0.7713$<br>Force: $F_{(3.784,37.84)} = 26.92$, $p < 0.0001$<br>Genotype: $F_{(1,10)} = 3.268$, $p = 0.1008$ | Bonferroni's multiple-comparisons test: WT vs KO<br>0.02 g: $p > 0.9999$<br>0.04 g: $p = 0.7634$<br>0.07 g: $p > 0.9999$<br>0.16 g: $p = 0.9983$<br>0.4 g: $p > 0.9999$<br>0.6 g: $p > 0.9999$<br>1.0 g: $p = 0.5572$ | Slurp2X WT: 6, Slurp2X KO: 6 |
| *2B* middle | Two-way ANOVA:<br>Force × genotype: $F_{(6,60)} = 1.273$, $p = 0.2832$<br>Force: $F_{(1.831,18.31)} = 97.79$, $p < 0.0001$<br>Genotype: $F_{(1,10)} = 14.55$, $p = 0.0034$ | Bonferroni's multiple-comparisons test: WT vs KO<br>0.02 g: $p = 0.4974$<br>0.04 g: $p = 0.0641$<br>0.07 g: $p = 0.0684$<br>0.16 g: $p = 0.0341$<br>0.4 g: $p = 0.0074$<br>0.6 g: $p = 0.0805$<br>1.0 g: $p = 0.2679$ | Slurp2X WT: 6, Slurp2X KO: 6 |
| *2B* bottom | Two-way ANOVA:<br>Force × genotype: $F_{(6,72)} = 3.934$, $p = 0.0019$<br>Force: $F_{(3.023,36.28)} = 73.03$, $p < 0.0001$<br>Genotype: $F_{(1,12)} = 13.14$, $p = 0.0035$ | Bonferroni's multiple-comparisons test: WT vs KO<br>0.02 g: $p = 0.1612$<br>0.04 g: $p = 0.0203$<br>0.07 g: $p > 0.9999$<br>0.16 g: $p = 0.0423$<br>0.4 g: $p = 0.0470$<br>0.6 g: $p = 0.0298$<br>1.0 g: $p = 0.0692$ | Slurp2X WT: 7, Slurp2X KO: 7 |
| *2C* | Two-way ANOVA:<br>Force × genotype: $F_{(6,228)} = 8.359$, $p < 0.0001$<br>Force: $F_{(5.112,194.2)} = 108.0$, $p < 0.0001$<br>Genotype: $F_{(1,38)} = 39.45$, $p < 0.0001$ | Bonferroni's multiple-comparisons test:<br>0.02 g: $p = 0.3780$<br>0.04 g: $p = 0.0357$<br>0.07 g: $p = 0.0096$<br>0.16 g: $p = 0.0419$<br>0.4 g: $p = 0.0004$<br>0.6 g: $p < 0.0001$<br>1.0 g: $p < 0.0001$ | Slurp1 WT: 20, Slurp1 KO: 20 |
| *2D* | Mann–Whitney nonparametric test<br>$p = 0.0005$ | | Slurp2X WT: 35, Slurp2X KO: 35 |
| *2E* | Mann–Whitney nonparametric test<br>$p = 0.0310$ | | Slurp1 WT: 16, Slurp1 KO: 16 |
| *2F* top left | Two-way ANOVA:<br>Force × genotype: $F_{(6,138)} = 11.71$, $p < 0.0001$<br>Force: $F_{(3.781,86.96)} = 80.01$, $p < 0.0001$<br>Genotype: $F_{(1,23)} = 39.91$, $p < 0.0001$ | Bonferroni's multiple-comparisons test: WT vs KO<br>0.02 g: $p = 0.1615$<br>0.04 g: $p = 0.0341$<br>0.07 g: $p > 0.9999$<br>0.16 g: $p = 0.0025$<br>0.4 g: $p < 0.0001$<br>0.6 g: $p = 0.0007$<br>1.0 g: $p = 0.0001$ | Slurp2X WT: 13, Slurp2X KO: 12 |
| *2F* top right | Two-way ANOVA:<br>Force × genotype: $F_{(6,150)} = 11.90$, $p < 0.0001$<br>Force: $F_{(4.293,107.3)} = 84.92$, $p < 0.0001$<br>Genotype: $F_{(1,25)} = 25.87$, $p < 0.0001$ | Bonferroni's multiple-comparisons test: WT vs KO<br>0.02 g: $p > 0.9999$<br>0.04 g: $p > 0.9999$<br>0.07 g: $p > 0.9999$<br>0.16 g: $p = 0.0447$<br>0.4 g: $p = 0.0087$<br>0.6 g: $p = 0.0002$<br>1.0 g: $p = 0.0001$ | Slurp2X WT: 13, Slurp2X KO: 14 |

(*Table continues.*)

**Table 1. Continued**

| Figure | Pre hoc | Post hoc | *N*, number of samples/animals per group |
|---|---|---|---|
| 2F bottom left | Two-way ANOVA:<br>Force × genotype: $F_{(6,180)} = 7.736$, $p < 0.0001$<br>Force: $F_{(4.955,148.7)} = 86.20$, $p < 0.0001$<br>Genotype: $F_{(1,30)} = 36.82$, $p < 0.0001$ | Bonferroni's multiple-comparisons test: WT vs KO<br>0.02 g: $p = 0.1889$<br>0.04 g: $p = 0.0492$<br>0.07 g: $p = 0.0261$<br>0.16 g: $p = 0.0298$<br>0.4 g: $p = 0.0015$<br>0.6 g: $p < 0.0001$<br>1.0 g: $p < 0.0001$ | Slurp1 WT: 16, Slurp1 KO: 16 |
| 2F bottom right | Two-way ANOVA:<br>Force × genotype: $F_{(6,36)} = 1.040$, $p = 0.4161$<br>Force: $F_{(2.500,15.00)} = 23.55$, $p < 0.0001$<br>Genotype: $F_{(1,6)} = 4.621$, $p = 0.0751$ | Bonferroni's multiple-comparisons test: WT vs KO<br>0.02 g: $p > 0.9999$<br>0.04 g: $p > 0.9999$<br>0.07 g: $p = 0.5347$<br>0.16 g: $p > 0.9999$<br>0.4 g: $p > 0.9999$<br>0.6 g: $p > 0.9999$<br>1.0 g: $p > 0.9999$ | Slurp1 WT: 4, Slurp1 KO: 4 |
| 3A | Mann–Whitney nonparametric test<br>Slurp2X $p < 0.0001$, Slurp1 $p < 0.0001$ | | Slurp2X WT: 30, Slurp2X KO: 30<br>Slurp1 WT: 27, Slurp1 KO: 26 |
| 3B | Mann–Whitney nonparametric test<br>Slurp2X $p = 0.002468$, Slurp1 $p = 0.001243$ | | Slurp2 WT: 8, Slurp2X KO: 9<br>Slurp1 WT: 8, Slurp1 KO: 7 |
| 3C | Two-way ANOVA:<br>Drug × genotype: $F_{(1,11)} = 6.632$, $p = 0.0258$<br>Drug: $F_{(1,11)} = 17.79$, $p = 0.0014$<br>Genotype: $F_{(1,11)} = 9.483$, $p = 0.0105$ | Bonferroni's multiple-comparisons test: WT vs KO<br>Capsaicin: $p = 0.0013$<br>Vehicle: $p > 0.9999$ | Slurp2X WT: 7, Slurp2X KO: 6 |
| 3D | Unpaired two-tailed Student's *t* test with Welch's correction<br>$t_{(28.87)} = 0.7596$, $p = 0.4536$ | | Slurp2X WT: 16, Slurp2X KO: 16 |
| 4A | Mann–Whitney nonparametric test | FDR = 5% correction using Benjamini, Krieger, and Yekutieli method<br>Slurp1: $q = 0.000182$<br>Slurp2X: $q = 0.000001$ | Slurp1 WT: 10, Slurp1 KO: 10<br>Slurp2X WT: 13, Slurp2X KO: 12 |
| 4B | Mann–Whitney nonparametric test | FDR = 5% correction using Benjamini, Krieger, and Yekutieli method<br>Slurp1: $q = 0.022019$<br>Slurp2X: $q = 0.000052$ | Slurp1 WT: 10, Slurp1 KO: 10<br>Slurp2X WT: 13, Slurp2X KO: 12 |
| 4C | Mann–Whitney nonparametric test | FDR = 5% correction using Benjamini, Krieger, and Yekutieli method<br>Slurp1: $q = 0.002455$<br>Slurp2X: $q = 0.001991$ | Slurp1 WT: 10, Slurp1 KO: 10<br>Slurp2X WT: 13, Slurp2X KO: 12 |
| 4D | Mann–Whitney nonparametric test | FDR = 5% correction using Benjamini, Krieger, and Yekutieli method<br>Slurp1: $q = 0.000580$<br>Slurp2X: $q = 0.000025$ | Slurp1 WT: 10, Slurp1 KO: 10<br>Slurp2X WT: 13, Slurp2X KO: 12 |
| 4E | Mann–Whitney nonparametric test | FDR = 5% correction using Benjamini, Krieger, and Yekutieli method<br>Slurp1: $q = 0.001334$<br>Slurp2X: $q = 0.034023$ | Slurp1 WT: 10, Slurp1 KO: 10<br>Slurp2X WT: 13, Slurp2X KO: 12 |
| 5A | Three-way ANOVA:<br>Genotype × drug: $F_{(1,22)} = 11.64$, $p = 0.0025$<br>Time × genotype × drug: $F_{(2,44)} = 9.612$, $p = 0.0003$<br>Two-way ANOVA:<br>Time: $F_{(1.678,73.82)} = 8.366$, $p = 0.0011$ | Tukey's multiple-comparisons test:<br>WT vehicle baseline vs WT indomethacin baseline: $p = 0.9971$<br>WT vehicle baseline vs KO vehicle baseline: $p < 0.0001$<br>WT indomethacin baseline vs KO indomethacin baseline: $p < 0.0001$<br>KO vehicle baseline vs KO indomethacin baseline: $p = 0.4735$<br>WT vehicle 30 min vs WT indomethacin 30 min: $p = 0.5697$<br>WT vehicle 30 min vs KO vehicle 30 min: $p < 0.0001$<br>WT indomethacin 30 min vs KO indomethacin 30 min: $p = 0.0002$<br>KO vehicle 30 min vs KO indomethacin 30 min: $p = 0.0030$<br>WT vehicle 2 h vs WT indomethacin 2 h: $p = 0.9849$ | Slurp2X WT: 12, Slurp2X KO: 12, same mice for vehicle and indomethacin |

(*Table continues.*)

**Table 1. Continued**

| Figure | Pre hoc | Post hoc | *N*, number of samples/animals per group |
|---|---|---|---|
| | | WT vehicle 2 h vs KO vehicle 2 h: $p < 0.0001$<br>WT indomethacin 2 h vs KO indomethacin 2 h: $p = 0.4687$<br>KO vehicle 2 h vs KO indomethacin 2 h: $p = 0.0007$<br>WT vehicle baseline vs WT vehicle 30 min: $p = 0.8476$<br>WT vehicle baseline vs WT vehicle 2 h: $p = 0.3824$<br>WT vehicle 30 min vs WT vehicle 2 h: $p = 0.1215$<br>WT indomethacin baseline vs WT indomethacin 30 min: $p = 0.7751$<br>WT indomethacin baseline vs WT indomethacin 2 h: $p = 0.8276$<br>WT indomethacin 30 min vs WT indomethacin 2 h: $p = 0.9912$<br>KO vehicle baseline vs KO vehicle 30 min: $p = 0.2475$<br>KO vehicle baseline vs KO vehicle 2 h: $p = 0.9994$<br>KO vehicle 30 min vs KO vehicle 2 h: $p = 0.1246$<br>KO indomethacin baseline vs KO indomethacin 30 min: $p = 0.0083$<br>KO indomethacin baseline vs KO indomethacin 2 h: $p = 0.0089$<br>KO indomethacin 30 min vs KO indomethacin 2 h: $p = 0.0595$ | |
| *5B* | Three-way ANOVA:<br>Genotype × drug: $F_{(1,22)} = 11.92$, $p = 0.0023$<br>Time × genotype × drug: $F_{(1,22)} = 0.06957$, $p = 0.7944$<br>Two-way ANOVA:<br>Time: $F_{(1,44)} = 0.3475$, $p = 0.5585$ | Tukey's multiple-comparisons test:<br>WT vehicle baseline vs WT indomethacin baseline: $p = 0.0402$<br>WT vehicle baseline vs KO vehicle baseline: $p = 0.0703$<br>WT indomethacin baseline vs KO indomethacin baseline: $p < 0.0001$<br>KO vehicle baseline vs KO indomethacin baseline: $p = 0.9959$<br>WT vehicle 3.5 h vs WT indomethacin 3.5 h: $p = 0.0220$<br>WT vehicle 3.5 h vs KO vehicle 3.5 h: $p = 0.9959$<br>WT indomethacin 3.5 h vs KO indomethacin 3.5 h: $p = 0.0041$<br>KO vehicle 3.5 h vs KO indomethacin 3.5 h: $p = 0.9866$<br>WT vehicle baseline vs WT vehicle 3.5 h: $p = 0.0494$<br>WT indomethacin baseline vs WT indomethacin 3.5 h: $p = 0.0992$<br>KO vehicle baseline vs KO vehicle 3.5 h: $p = 0.1847$<br>KO indomethacin baseline vs KO indomethacin 3.5 h: $p = 0.2447$ | Slurp2X WT: 12, Slurp2X KO: 12, same mice for vehicle and indomethacin |
| *5C* | Three-way ANOVA:<br>Genotype × drug: $F_{(1,36)} = 4.191$, $p = 0.0480$<br>Time × genotype × drug: $F_{(1,36)} = 1.005$, $p = 0.3228$<br>Two-way ANOVA:<br>Time: $F_{(1,36)} = 0.8802$, $p = 0.3544$ | Tukey's multiple-comparisons test:<br>WT vehicle baseline vs WT gabapentin baseline: $p = 0.8387$<br>WT vehicle baseline vs KO vehicle baseline: $p < 0.0001$<br>WT gabapentin baseline vs KO gabapentin baseline: $p < 0.0001$<br>KO vehicle baseline vs KO gabapentin baseline: $p = 0.9020$<br>WT vehicle 30 min vs WT gabapentin 30 min: $p = 0.6952$ | Slurp2X WT vehicle: 10, Slurp2X WT gabapentin: 10, Slurp2X KO vehicle: 10, Slurp2X KO gabapentin: 10 |

(*Table continues.*)

**Table 1. Continued**

| Figure | Pre hoc | Post hoc | *N*, number of samples/animals per group |
|---|---|---|---|
| | | WT vehicle 30 min vs KO vehicle 30 min: $p = 0.0520$<br>WT gabapentin 30 min vs KO gabapentin 30 min: $p < 0.0001$<br>KO vehicle 30 min vs KO gabapentin 30 min: $p = 0.1679$<br>WT vehicle baseline vs WT gabapentin 30 min: $p = 0.1660$<br>WT vehicle baseline vs WT gabapentin 30 min: $p = 0.2788$<br>KO vehicle baseline vs KO gabapentin 30 min: $p = 0.0044$<br>KO vehicle baseline vs KO gabapentin 30 min: $p = 0.1856$ | |
| 5D | Three-way ANOVA:<br>Genotype × drug: $F_{(1,36)} = 11.14$, $p = 0.0020$<br>Time × genotype × drug: $F_{(1,36)} = 9.601$, $p = 0.0038$<br>Two-way ANOVA:<br>Time: $F_{(1,36)} = 14.74$, $p = 0.0005$ | Tukey's multiple-comparisons test:<br>WT vehicle baseline vs WT gabapentin baseline: $p > 0.9999$<br>WT vehicle baseline vs KO vehicle baseline: $p = 0.9988$<br>WT gabapentin baseline vs KO gabapentin baseline: $p = 0.9697$<br>KO vehicle baseline vs KO gabapentin baseline: $p = 0.9469$<br>WT vehicle 30 min vs WT gabapentin 30 min: $p < 0.0001$<br>WT vehicle 30 min vs KO vehicle 30 min: $p = 0.9575$<br>WT gabapentin 30 min vs KO gabapentin 30 min: $p < 0.0001$<br>KO vehicle 30 min vs KO gabapentin 30 min: $p = 0.9469$<br>WT vehicle baseline vs WT gabapentin 30 min: $p = 0.6927$<br>WT vehicle baseline vs WT gabapentin 30 min: $p < 0.0001$<br>KO vehicle baseline vs KO gabapentin 30 min: $p = 0.9825$<br>KO vehicle baseline vs KO gabapentin 30 min: $p = 0.2619$ | Slurp2X WT vehicle: 10, Slurp2X WT gabapentin: 10, Slurp2X KO vehicle: 10, Slurp2X KO gabapentin: 10 |
| 6A | Two-way ANOVA:<br>Time × drug: $F_{(1,20)} = 1.956$, $p = 0.1772$<br>Time: $F_{(1,20)} = 0.8599$, $p = 0.3648$<br>Drug: $F_{(1,20)} = 5.316 \times 10^{-5}$, $p = 0.9943$ | Bonferroni's multiple-comparisons test: vehicle vs indomethacin<br>Baseline: $p = 0.6851$<br>2 h post: $p = 0.6746$ | Vehicle: 11, indomethacin: 11, same mice |
| 6B | Two-way ANOVA:<br>Time × drug: $F_{(1,20)} = 4.756$, $p = 0.0413$<br>Time: $F_{(1,20)} = 0.002937$, $p = 0.9573$<br>Drug: $F_{(1,20)} = 0.09109$, $p = 0.7659$ | Bonferroni's multiple-comparisons test: vehicle vs indomethacin<br>Baseline: $p = 0.2891$<br>2 h post: $p = 0.1368$ | Vehicle: 11, indomethacin: 11, same mice |
| 6C | Two-way ANOVA:<br>Time × drug: $F_{(1,20)} = 6.589$, $p = 0.0184$<br>Time: $F_{(1,20)} = 1.695$, $p = 0.2077$<br>Drug: $F_{(1,20)} = 2.020$, $p = 0.1707$ | Bonferroni's multiple-comparisons test: vehicle vs indomethacin<br>Baseline: $p = 0.0234$<br>2 h post: $p > 0.9999$ | Vehicle: 11, indomethacin: 11, same mice |
| 6D | Two-way ANOVA:<br>Time × drug: $F_{(1,20)} = 0.3361$, $p = 0.5686$<br>Time: $F_{(1,20)} = 0.5510$, $p = 0.4665$<br>Drug: $F_{(1,20)} = 0.3361$, $p = 0.5686$ | Bonferroni's multiple-comparisons test: vehicle vs indomethacin<br>Baseline: $p = 0.8439$<br>2 h post: $p > 0.9999$ | Vehicle: 11, indomethacin: 11, same mice |
| 6E | Two-way ANOVA:<br>Time × drug: $F_{(1,20)} = 0.5158$, $p = 0.4810$<br>Time: $F_{(1,20)} = 12.89$, $p = 0.0018$<br>Drug: $F_{(1,20)} = 2.997$, $p = 0.0988$ | Bonferroni's multiple-comparisons test: vehicle vs indomethacin<br>Baseline: $p = 0.1863$<br>2 h post: $p = 0.9908$ | Vehicle: 11, indomethacin: 11, same mice |
| 7B | Unpaired two-tailed Student's *t* test with Welch's correction.<br>CD68: $t_{(5.559)} = 2.978$, $p = 0.0271$<br>CD3: $t_{(6.290)} = 5.733$, $p = 0.001038$<br>Avidin: $t_{(8.490)} = 11.90$, $p = 0.000001$<br>CD207: $t_{(6.511)} = 7.755$, $p = 0.000161$ | | CD68 and CD3: Slurp2X WT: 6, Slurp2X KO: 6.<br>Avidin and CD207: Slurp2X WT: 5, Slurp2X KO: 6 |

(*Table continues.*)

**Table 1. Continued**

| Figure | Pre hoc | Post hoc | *N*, number of samples/animals per group |
|---|---|---|---|
| 8A | Multiple unpaired two-tailed Student's *t* test with Welch's correction<br>Slurp2X pad PGP9.5: $p = 0.644805$, $q = 0.750812$<br>Slurp2X pad CGRP: $p = 0.743378$, $q = 0.750812$<br>Slurp2X glabrous PGP9.5: $p = 0.011020$, $q = 0.022261$<br>Slurp2X glabrous CGRP: $p = 0.067195$, $q = 0.067867$ | | Slurp2X WT: 8, Slurp2X KO: 8 |
| 8B | Multiple Mann–Whitney nonparametric test<br>Slurp1 GFRa2/IB4: $p = 0.818182$, $q = 0.826364$<br>Slurp1 GFRa2/CGRP(Br): $p = 0.454545$, $q = 0.688636$<br>Slurp1 GFRa2/CGRP(Dim): $p = 0.125541$, $q = 0.380390$<br>Slurp1 IB4/CGRP(Br): $p = 0.3209004$, $q = 0.332294$<br>Slurp1 IB4/CGRP(Dim): $p = 0.240260$, $q = 0.332294$ | | Slurp1 WT: 6, Slurp1 KO: 6 |
| 8C | Multiple Mann–Whitney nonparametric test<br>Slurp2X pad GFRa2: $p = 0.798446$, $q > 0.999999$<br>Slurp2X pad CGRP: $p = 0.130381$, $q = 0.395054$<br>Slurp2X pad GFRa2/CGRP: $p > 0.999999$, $q > 0.999999$<br>Slurp2X glabrous GFRa2: $p = 0.001088$, $q = 0.002197$<br>Slurp2X glabrous CGRP: $p = 0.234499$, $q = 0.157896$<br>Slurp2X glabrous GFRa2/CGRP: $p = 0.020668$, $q = 0.020875$ | | Slurp2X WT: 8, Slurp2X KO: 8 |
| 9B | Chi-square test.<br>$p = 0.0004$ | | Slurp2X WT: 2/24 neurons, Slurp2X KO: 12/21 neurons |
| 9D | Unpaired two-tailed Student's *t* test.<br>$p = 0.0015$ | | Slurp2X WT: 22 neurons, Slurp2X KO: 9 neurons |
| 9E,F | Unpaired two-tailed Student's *t* test.<br>E: $p = 0.7449$<br>F: $p = 0.8415$<br>G: $p = 0.9816$<br>H: $p = 0.4501$ | | Slurp2X WT: 22 neurons, Slurp2X KO: 9 neurons |
| 10C | Chi-squared test<br>$p = 0.0343$ | | Slurp2X WT: 0/15 neurons, Slurp2X KO: 7/29 neurons |
| 10E | Two-way ANOVA:<br>Force × genotype: $F_{(3,99)} = 5.393$, $p = 0.0018$<br>Force: $F_{(3,99)} = 67.96$, $p < 0.0001$<br>Genotype: $F_{(1,33)} = 34.6$, $p < 0.0001$ | Bonferroni's multiple-comparisons test: WT vs KO<br>5 mN: $p = 0.1426$<br>10 mN: $p < 0.0001$<br>20 mN: $p < 0.0001$<br>40 mN: $p < 0.0001$ | Slurp2X WT: 12 neurons Slurp2X KO: 21 neurons |
| 10F | Unpaired two-tailed Student's *t* test.<br>$p = 0.5621$ | | Slurp2X WT: 12 neurons Slurp2X KO: 25 neurons |

ganglia. As expected, reverse transcription polymerase chain reaction (RT-PCR) of cDNA from paw skin of wild-type mice revealed robust expression of mRNAs encoding both proteins. RT-PCR of wild-type lumbar DRG revealed barely detectable expression of Slurp1 mRNA but more substantial expression of Slurp2 mRNA (Fig. 1*C*).

### Slurp1 KO and Slurp2X KO mice exhibit multimodal evoked pain hypersensitivity

To evaluate the sensory phenotype of the Slurp1 KO and Slurp2X KO mice, we conducted behavioral assays targeting mechanical, thermal, and chemical nociception. To assess punctate mechanical sensitivity, we applied a range of forces to the hindpaw glabrous skin using von Frey filaments. Slurp2X KO mice on a mixed C57Bl/6J and SVE-129 background displayed a significant increase in hindpaw withdrawal from mechanical stimulation, compared with wild-type controls, at 0.04 and 0.16–1 g (Fig. 2*A*). Although a cohort of Slurp2X KO mice backcrossed 10 generations onto a C57Bl/6J background exhibited only a trend in mechanical hypersensitivity when assayed by the same investigator, reassay of this second cohort by a second experimenter confirmed the augmented mechanical hypersensitivity, as did evaluation of an additional cohort of backcrossed Slurp2X KO mice by a third investigator (Fig. 2*B*). Similarly, Slurp1 KO mice on a C57Bl/6J background displayed a significant increase in percent withdrawal from stimulation at 0.04–1 g (Fig. 2*C*) as compared with wild type. To corroborate these findings, we assayed von Frey filament responses in both Slurp2X KO and Slurp1 KO mice, each on the C57Bl/6J background, using the up-down method, to interpolate a 50% withdrawal threshold. This approach also revealed enhanced mechanical sensitivity in both Slurp1 knock-out and Slurp2X knock-out mice (Fig. 2*D*,*E*).

To test heat pain sensitivity, noxious radiant heat stimulation was applied to the hindpaw glabrous skin. Both Slurp2X KO and Slurp1 KO mice exhibited shorter latencies to paw withdrawal than wild-type mice (Fig. 3*A*). In order to assess whether this thermal hypersensitivity extended to the front paw, noxious laser stimuli (445 nm, 200 mW) were applied to the glabrous front paw skin. Both Slurp2X KO and Slurp1 KO mice displayed shortened withdrawal latencies following front paw stimulation, consistent with our findings for the hindpaw (Fig. 3*B*). To rule out sex differences in behavioral pain responses, male and female

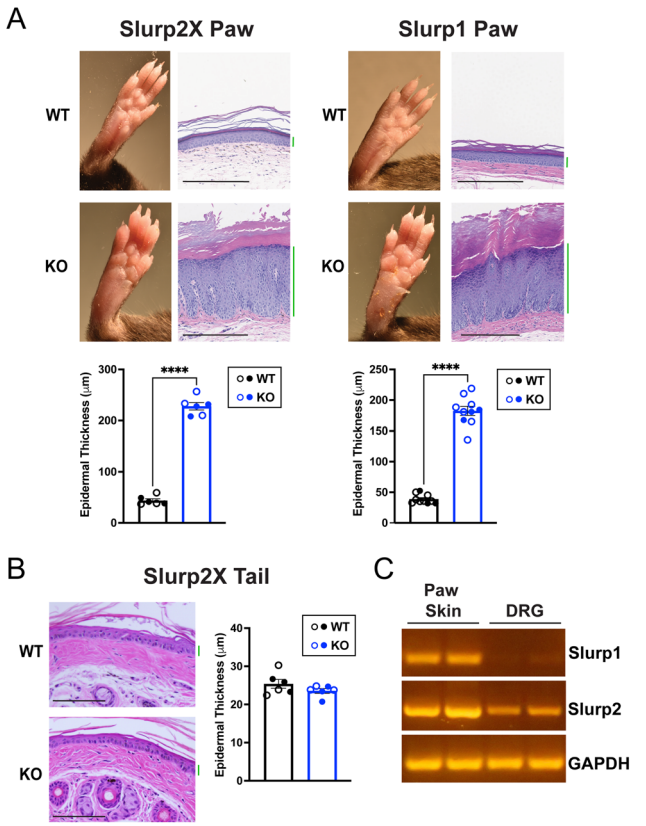


**Figure 1.** Slurp2X KO and Slurp1 KO mice display PPK. ***A***, Representative macroscopic and H&E images of hindpaw plantar skin of Slurp2X (left) and Slurp1 (right) knock-out (KO, blue, $n = 6$ for Slurp2X, $n = 10$ for Slurp1) mice and wild-type (WT, black, $n = 6$ for Slurp2X, $n = 10$ for Slurp1) controls. Scale bar = 250 µm. Epidermal thickness of the hindpaw glabrous skin (green bars to right of photos) is plotted at bottom. Unpaired two-tailed Student's *t* test with Welch's correction, $****p < 0.0001$. ***B***, Representative H&E images of tail skin of Slurp2X KO (KO, blue, $n = 6$) mice and wild-type (WT, black, $n = 6$) controls. Scale bar = 100 µm. Epidermal thickness of the tail skin is plotted at the bottom. Unpaired two-tailed Student's *t* test with Welch's correction. In all panels, bar graphs show mean ± SEM, and data points represent individual female (open circles) and male (filled circles) mice. Epidermis thickness was quantified on Slurp2X mice and Slurp1 mice on a C57/Bl6 background. ***C***, RT-PCR analysis of Slurp mRNA expression in paw skin and lumbar DRGs of wild-type mice. Amplification products are from four different mice.

mice of each genotype were analyzed separately for the von Frey (Fig. 2*F*) and thermal analyses (Fig. 3, open and filled circles, respectively). Neither assay showed obvious sex differences. Slurp1 KO and Slurp2X KO mice of both sexes had significantly shorter latencies to withdrawal from a hindpaw heat stimulus. Both male and female Slurp2X KO mice displayed significant mechanical hypersensitivity at multiple forces. Slurp1 KO male mice were hypersensitive at multiple von Frey forces. An inadequate number of Slurp1 KO female mice were assayed for mechanical sensitivity to reach significance; however, they displayed a similar trend.

To determine whether chemical nociception was altered by SLURP2 knock-out, we subcutaneously injected hindpaws of Slurp2X KO mice and wild-type controls with capsaicin (1 µg in 10 µl) and vehicle in alternate paws. The licking response to vehicle alone was unchanged between Slurp2X KO and wild-type mice. However, the licking response to a capsaicin injection in the opposite paw 48 h later was significantly greater in the Slurp2X KO animals (Fig. 3*C*). Capsaicin sensitivity was not assessed in Slurp1 KO mice.

These data strongly suggest that stimulating regions of PPK produces a heightened pain response in Slurp1 KO and Slurp2X KO mice. To determine if this sensory phenotype was linked to the PPK or was a more global result of the genetic mutations, especially given the expression of Slurp2 in DRG, we evaluated the sensory phenotype of these animals in the tail skin, which displays no macroscopically evident PPK. The tails of Slurp2X KO mice and wild-type controls were partially immersed in a 48°C water bath until the mice flicked their tail out of the water. There was no difference in tail withdrawal responses between genotypes, arguing against thermal hyperalgesia in the tail (Fig. 3*D*) and suggesting that the absence of Slurp2 from sensory ganglia, per se, is insufficient to establish a state of thermal hyperalgesia in skin regions lacking PPK.

### Slurp1 KO and Slurp2X KO mice exhibit spontaneous pain-associated behaviors

To determine if Slurp1 KO and Slurp2X KO mice displayed any signs of nonevoked pain sensation, we video recorded mice in observation boxes for 10 min and scored paw flinching, paw withdrawal, paw licking, and time spent resting on the front paws. Slurp2X KO and Slurp1 KO mice spent significantly more time with their front paws withdrawn close to their body and less time with their front paws resting flat on the glass (Fig. 4*A*,*B*). Additionally, Slurp2X KO and Slurp1 KO mice both exhibited increased episodes of flinching, front paw licking, and hindpaw licking compared with wild-type controls (Fig. 4*C*–*E*). These results indicate that Slurp2X KO and Slurp1 KO mice experience discomfort even without provocation from experimenter-applied stimuli.

Collectively, these data suggest a multimodal behavioral hypersensitivity isolated to the affected palmoplantar region of Slurp1 KO and Slurp2X KO animals. Given the similarities between these two knock-out models, subsequent experiments were performed only with Slurp2X KO mice.

### Indomethacin, but not gabapentin, alleviates thermal hypersensitivity in Slurp2X KO mice

Individuals experiencing pain in conjunction with their PPK often seek relief through nonsteroidal anti-inflammatory drugs (NSAIDs; Milstone et al., 2005). To evaluate the effects of NSAIDs on Slurp2X KO mice, we injected mice with indomethacin (10 mg/kg, i.p.) and conducted evoked behavioral analysis at ~30 min, ~2 h, and ~3.5 h postinjection. Three-way ANOVA confirmed an overall statistically significant interaction of treatment and genotype in both assays. In order to determine what was driving this statistically significant interaction of treatment and genotype, we further analyzed each experimental groups using two-way ANOVA. Indomethacin injections significantly increased the withdrawal latencies to noxious heat stimulation in Slurp2X KO mice, whereas mice injected with vehicle showed no difference in withdrawal latencies from baseline (Fig. 5*A*). Withdrawal frequency in response to a 1 g mechanical stimulation did not differ between indomethacin treatment and vehicle controls in Slurp2X KO mice (Fig. 5*B*). Interestingly, in wild-type mice, indomethacin produced a slight decrease in withdrawal from mechanical stimulation but no significant change in thermal response latency (Fig. 5*A*,*B*). When we analyzed spontaneous behaviors after indomethacin treatment, we found no significant effects of the drug on front paw withdrawal, front paw licking, hindpaw licking, or flinching behaviors (Fig. 6*A*–*E*). These results reveal that cyclooxygenase inhibition can provide temporary relief from the thermal hypersensitivity, but may not

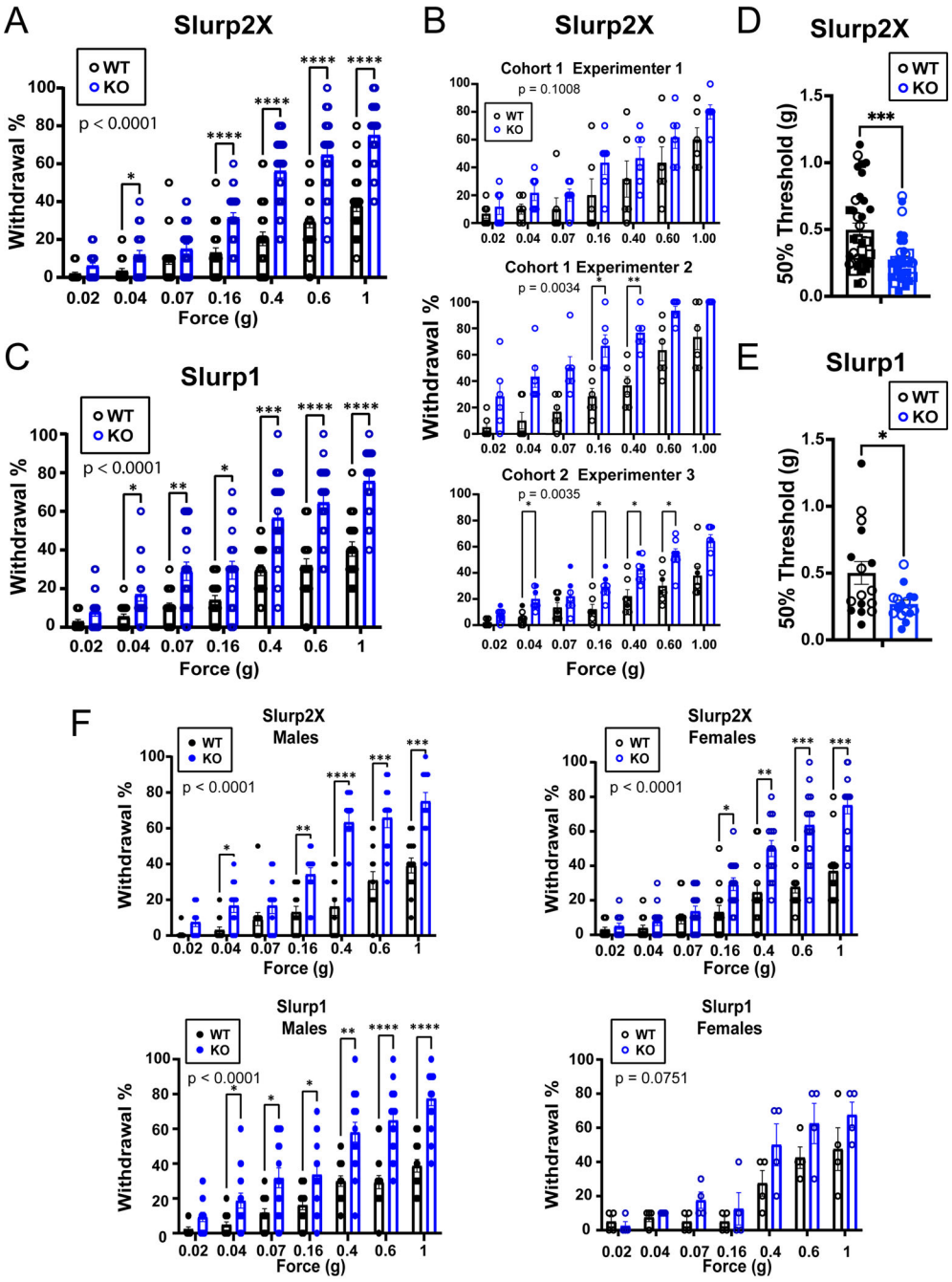


**Figure 2.** Slurp2X KO and Slurp1 KO mice display increased mechanically evoked pain-related behaviors. ***A***, Frequency of withdrawal from von Frey filaments in hindpaw plantar skin in Slurp2X KO mice (KO, blue, $n = 26$) and wild-type controls (WT, black, $n = 26$). Two-way ANOVA with Bonferroni's correction, $*p < 0.05$, $****p < 0.0001$. The majority of these mice were on a mixed SVE-129 and C57Bl6 background. ***B***, Top, Frequency of withdrawal from von Frey filaments in hindpaw plantar skin of Slurp2X KO female mice (KO, blue, $n = 6$) and wild-type controls (WT, black, $n = 6$) backcrossed 10 generations onto the C57Bl6 background (10 total stimulations per force). Middle, Withdrawal frequency in the same cohort of animals assayed by a second investigator. Bottom, Withdrawal frequency of a subsequent cohort of backcrossed animals (8–12 generations) assessed by an independent investigator (20 total stimulations per force), two-way ANOVA with Bonferroni's correction, $*p < 0.05$, $**p < 0.01$. ***C***, Von Frey filament 50% withdrawal threshold in Slurp1 KO mice (blue, $n = 20$) and wild-type controls (black, $n = 20$) on a C57Bl6 background (two-way ANOVA with Bonferroni's correction, $*p < 0.05$, $**p < 0.01$, $***p < 0.001$, $****p < 0.0001$). ***D***, Von Frey filament 50% withdrawal threshold in a separate group of Slurp2X KO mice (KO, blue, $n = 35$) and wild-type controls (WT, black, $n = 35$) on a C57Bl6 background, assayed using the up-down method. Squares represent the mice that were further used for the gabapentin experiment in Figure 5. Mann–Whitney nonparametric test, $***p < 0.001$. ***E***, Von Frey filament 50% withdrawal threshold in a separate group of Slurp1 KO mice (KO, blue, $n = 16$) and wild-type controls (WT, black, $n = 16$) on a C57Bl6 background, assayed using the up-down method. Mann–Whitney nonparametric test, $*p < 0.05$. ***F***, Mechanical sensitivity data from panels ***A*** and ***C***, reanalyzed by sex. Each graph shows frequency of withdrawal from von Frey filaments in hindpaw plantar skin Top left, Slurp2X KO male mice (KO, blue, $n = 12$) and wild-type controls (black, $n = 13$). Top right, Slurp2X KO female mice (KO, blue, $n = 14$) and wild-type controls (WT, black, $n = 13$). Bottom left, Slurp1 KO male mice (KO, blue, $n = 16$) and wild-type controls (WT, black, $n = 16$). Bottom right, Slurp1 KO female mice (KO, blue, $n = 4$) and wild-type controls (WT, black, $n = 4$). Statistical analysis performed with two-way ANOVA with Bonferroni's correction, $*p < 0.05$, $**p < 0.01$, $***p < 0.001$, $****p < 0.0001$. In all panels, bar graphs show mean ± SEM, and data points represent individual female (open circles) and male (filled circles) mice.

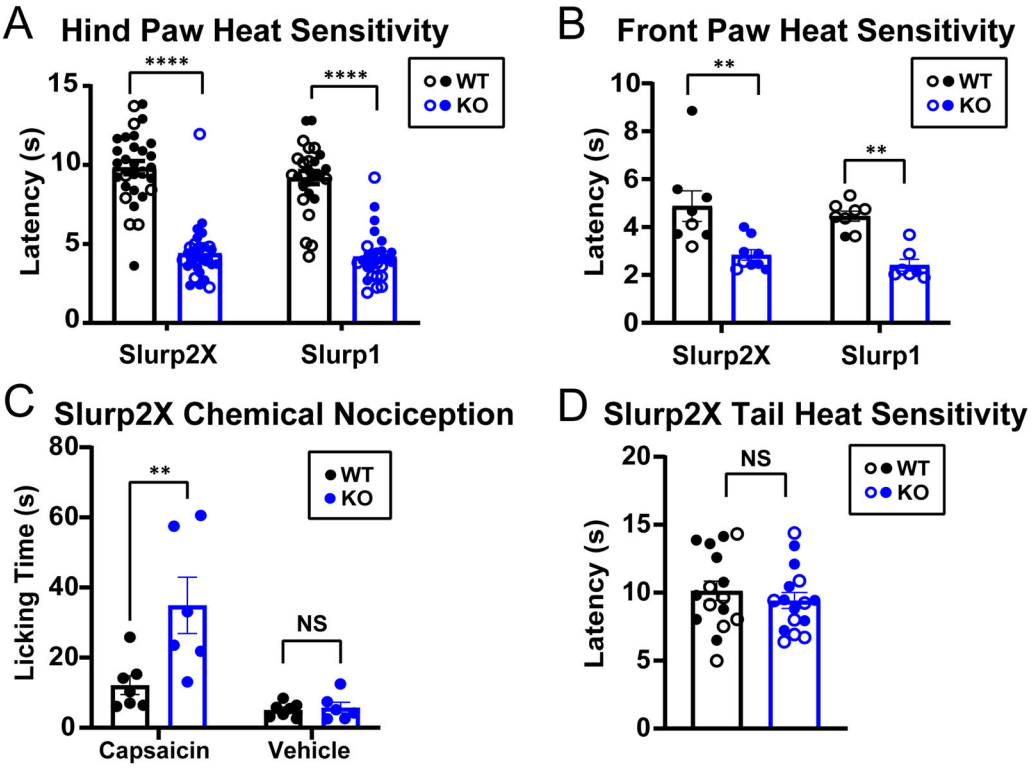


**Figure 3.** Slurp2X KO and Slurp1 KO mice display increased heat- and capsaicin-evoked pain-related behaviors in PPK-affected skin. ***A***, Latency of withdrawal from radiant heat stimuli in hindpaw plantar skin in Slurp2X KO mice ($n = 30$) and wild-type controls ($n = 30$) and in Slurp1 KO mice ($n = 26$) and wild-type controls ($n = 27$). Mann–Whitney nonparametric test, $****p < 0.0001$. ***B***, Latency of withdrawal from laser heat stimulation of front paw plantar skin in Slurp2X KO mice ($n = 9$) and wild-type controls ($n = 8$) and in Slurp1 KO mice ($n = 7$) and wild-type controls ($n = 8$). Mann–Whitney nonparametric test, $**p < 0.01$. ***C***, Total paw licking time over 10 min after subcutaneous injection with capsaicin (1 µg) or vehicle alone into male Slurp2X KO mice ($n = 6$) and wild-type controls ($n = 7$). Two-way ANOVA with Bonferroni's correction, $**p < 0.01$. ***D***, Latency to tail withdrawal from a heated water bath in Slurp2X KO mice ($n = 16$) and wild-type controls ($n = 16$). No significant difference, unpaired two-tailed Student's $t$ test with Welch's correction. In all panels, bar graphs show mean ± SEM, and data points represent individual female (open circles) and male (filled circles) mice. The majority of Slurp2X mice evaluated were on a mixed SVE-129 and C57/Bl6 background while Slurp1 mice were on a C57/Bl6 background.

affect mechanical sensitivity or spontaneous pain behaviors, in Slurp2X KO mice.

Gabapentin is a drug commonly used for treatment of neuropathic pain. Following assessment of baseline heat and mechanical behavioral sensitivity, we injected Slurp2X KO and wild-type mice with gabapentin (100 mg/kg, i.p.) or vehicle and analyzed behaviors at ∼30 min (heat) and ∼2 h (mechanical) postinjection. Three-way ANOVA confirmed an overall statistically significant interaction of treatment and genotype in both assays. In order to determine what was driving this statistically significant interaction of treatment and genotype, we further analyzed each experimental group using two-way ANOVA. Gabapentin injections did not significantly alter the 50% withdrawal threshold to mechanical stimuli or the withdrawal latency to noxious heat stimuli in Slurp2X KO mice (Fig. 5*C*,*D*). However, we did observe a small but significant elevation of heat-response latency in vehicle-injected Slurp2X KO mice (Fig. 5*C*). In contrast, gabapentin injection significantly increased the 50% withdrawal threshold in wild-type mice, whereas mice injected with vehicle showed no apparent difference in withdrawal threshold from baseline (Fig. 5*D*). Neither gabapentin nor vehicle produced a significant change in withdrawal latency to noxious heat in wild-type mice (Fig. 5*C*). However, in this specific experiment, no apparent difference in baseline mechanosensitivity was observed between wild-type and Slurp2X KO mice, even though a lower mechanical threshold had been observed in the same cohort of mice ∼2 weeks prior to the pharmacological experiment (Fig. 2*D*). This inconsistency might be attributable to variable conditions on the days of these experiments. Regardless, these results suggest that gabapentin does not attenuate either heat or mechanical sensitivity in Slurp2X KO mice.

**Slurp2X KO mice have alterations in cutaneous immune cells**

SLURP1 is known to be expressed on immune cells and is an important factor in T-cell activation and function (Tjiu et al., 2011). Additionally, immune cells can release a variety of factors that can sensitize nociceptive neurons (Pinho-Ribeiro et al., 2017; Totsch and Sorge, 2017). Alterations in immune cells have been reported in the keratin 16 knock-out model of Pachyonychia Congenita (PC; Lessard et al., 2013) as well as in human patients with Olmsted syndrome (OS) and MdM (Danso-Abeam et al., 2013; Kudo et al., 2020). We therefore examined selected immune cell populations within the PPK-affected plantar skin of Slurp2X KO mice. Immunohistochemical staining of Slurp2X KO hindpaw plantar skin revealed significant alterations in the abundance of multiple classes of immune cells (Fig. 7*A*,*B*). These alterations included ∼5-fold increases in the number of $CD3^+$ T-cells and $CD68^+$ macrophages, and a fourfold increase in $Avidin^+$ cells that are presumably mast cells (Green et al., 2019). Whereas the increased macrophages and mast cells were evident throughout the dermis, the increase in T-cells was most evident in the vicinity of the dermal papillae, which are exaggerated in PPK-affected skin. Conversely, we observed a threefold decrease in epidermal Langerhans cells (CD207) in

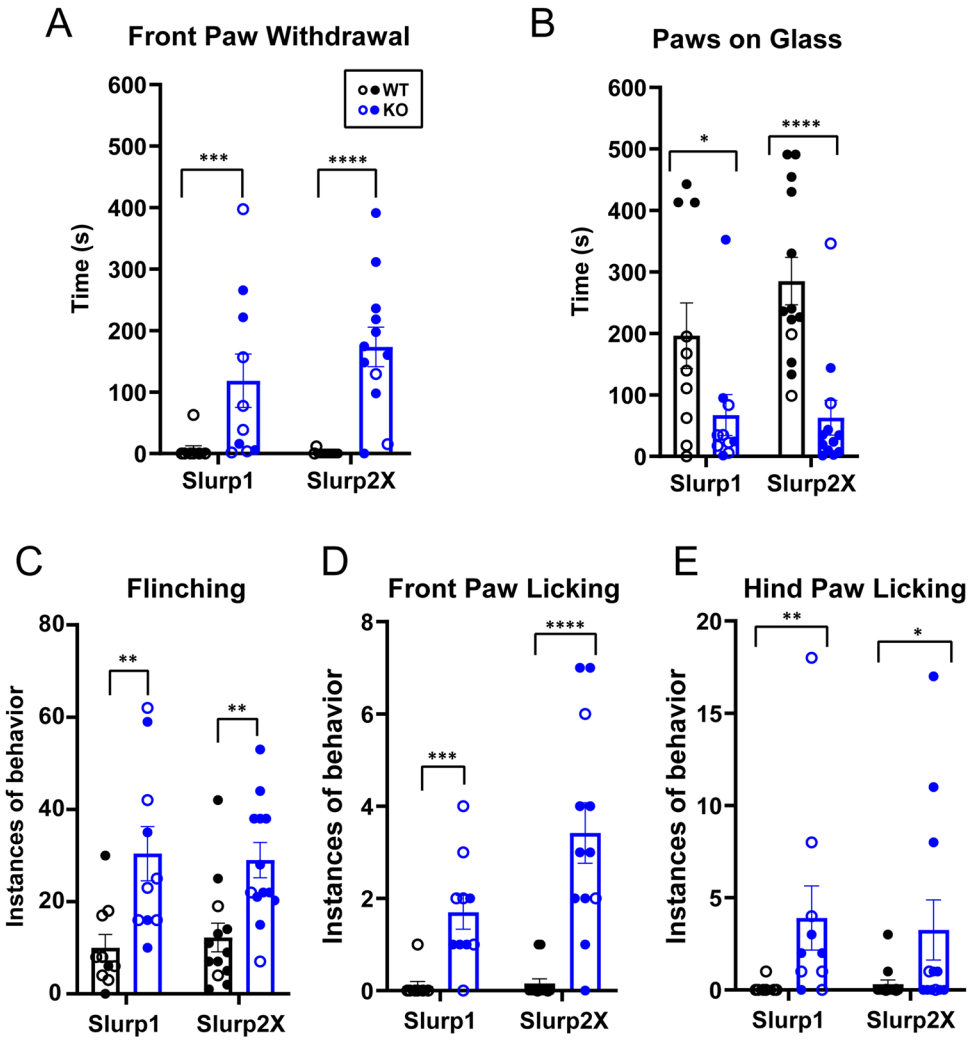


**Figure 4.** Slurp2X KO and Slurp1 KO mice display spontaneous pain behaviors. ***A–E***, Spontaneous pain behaviors measured across 10 min of Slurp1 KO and Slurp2X KO mice compared with wild-type controls. ***A***, Time the animal kept a front paw withdrawn close to the body. ***B***, Time the animal kept both front paws flat on the glass surface. ***C***, Instances of front paw flinching behavior. ***D***, Instances of front paw licking behavior. ***E***, Instances of hindpaw licking behavior. All statistical analysis performed using Mann–Whitney with FDR = 5% correction using Benjamini, Krieger, and Yekutieli method, $*q < 0.05$, $**q < 0.01$, $***q < 0.001$, $****q < 0.0001$. In all panels, Slurp1 KO ($n = 10$), Slurp1 wild-type controls ($n = 10$), Slurp2X KO mice ($n = 12$), Slurp2X wild-type controls ($n = 13$). Bar graphs show mean ± SEM, and data points represent individual female (open circles) and male (filled circles) mice. The majority of mice evaluated were backcrossed at least 8 generations on a C57Bl/6J background.

the hindpaws of Slurp2X KO mice. These results suggest that Slurp2X KO mice exhibit an altered immune cell profile in regions of PPK.

### Palmoplantar epidermal nerve fiber density in Slurp2X KO mice

Epidermal nerve fiber density is often altered in painful disorders (Polydefkis et al., 2004; Mellgren et al., 2013; Schuttenhelm et al., 2015). To determine whether the changes in pain behavior in Slurp2X KO mice might also be associated with alterations in epidermal neuroanatomy, we first stained hindpaw pad skin and glabrous skin for the pan-neuronal marker PGP9.5 and for the peptidergic sensory neuron marker calcitonin gene-related peptide (CGRP). In pad skin, Slurp2X KO mice exhibited no differences in IENFD compared with wild-type controls (Fig. 8*A*) for either PGP9.5- or CGRP-labeled fibers. In glabrous skin, there was a trend toward reduced IENFD for both markers that did not reach statistical significance. To further explore this issue and to expand our analysis of neuronal subtypes, we performed immunofluorescence staining on pad and glabrous skin. Once again, we used CGRP as a marker of peptidergic fibers. Although the Isolectin B4 (IB4) binding is a commonly used marker of nonpeptidergic neuronal cell bodies in DRGs, it does not exhibit the necessary specificity of staining in skin to be useful for this purpose. We therefore instead used antibodies against glial cell line-derived neurotrophic factor family receptor alpha 2 (GFRα2), which has been reported to exhibit substantial overlap with IB4. To validate the use of this marker, we first costained DRGs of wild-type and Slurp2X KO mice with anti-CGRP, anti-GFRα2, and fluorescently labeled IB4. As previously reported (Bennett et al., 1998; Lindfors et al., 2006; Jeon et al., 2024), there was substantial overlap between GFRα2 and IB4 labeling. Strongly CGRP-positive neurons tended to be negative for both GFRα2 and IB4 (Fig. 8*B*). However, as we recently observed (Jeon et al., 2024), some CGRP/GFRα2 double labeling and some CGRP/IB4 double labeling were seen, albeit predominantly in cells that showed only weak or fragmented CGRP staining (Fig. 8*B*). These findings thus confirm that the majority of GFRα2-positive cells are likely to be

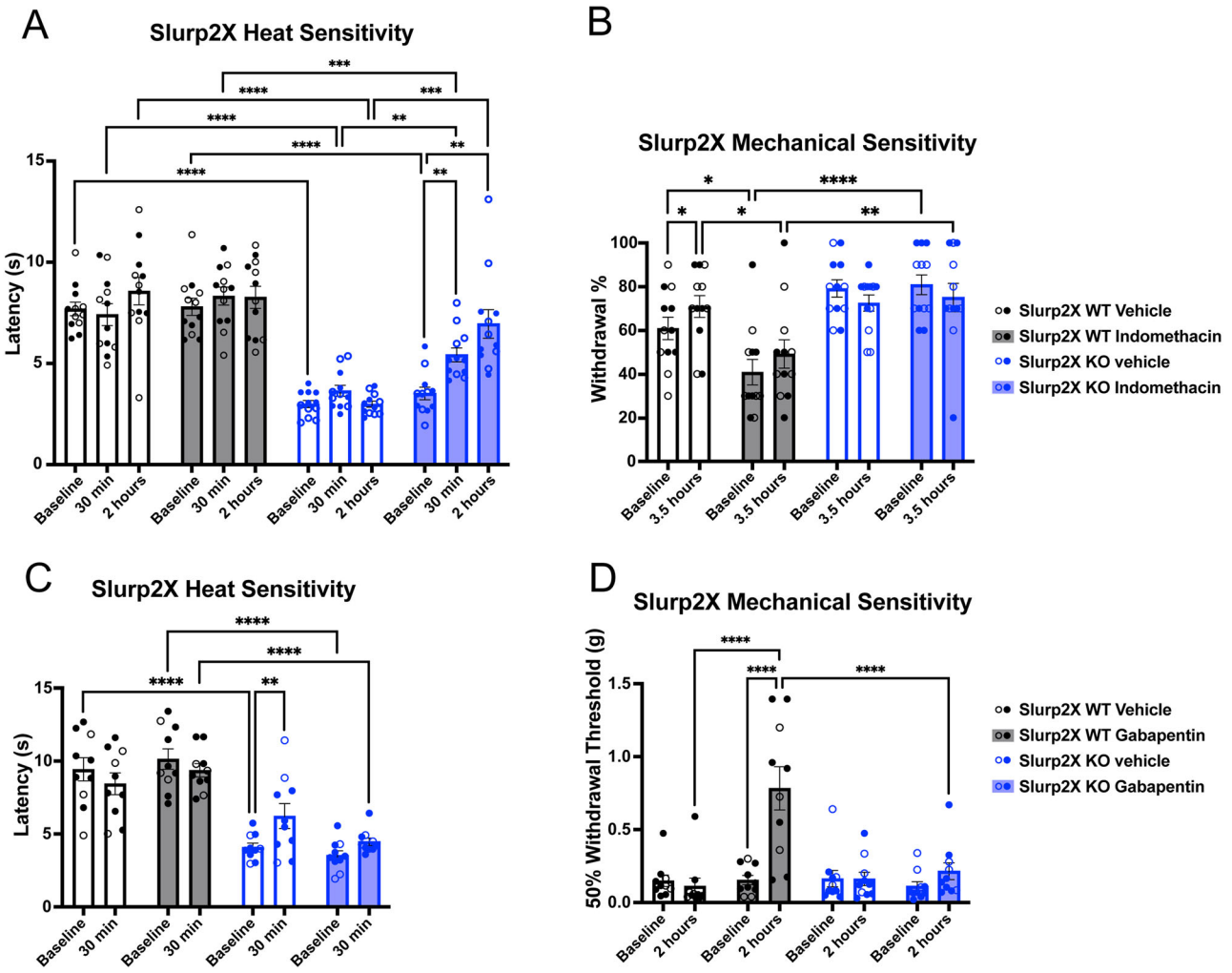


**Figure 5.** Indomethacin, but not gabapentin, alleviates thermal hypersensitivity in Slurp2X KO mice. ***A***, ***B***, Mechanical and thermal sensitivity of Slurp2X KO mice before and after indomethacin treatment as compared with wild-type controls. ***A***, Latency of withdrawal from radiant heat stimuli in hindpaw plantar skin in Slurp2X wild-type mice at baseline and after vehicle (black, clear bar, $n = 12$) or indomethacin (blue, clear bar, $n = 12$) injection and Slurp2X KO mice ($n = 12$) at baseline and after vehicle (black, gray bar, $n = 12$) or indomethacin (blue, light blue bar, $n = 12$) injection. ***B***, Frequency of withdrawal from a 1.0 g von Frey filament in hindpaw plantar skin in Slurp2X wild-type mice at baseline and after vehicle (black, clear bar, $n = 12$) or indomethacin (blue, clear bar, $n = 12$) injection and Slurp2X KO mice ($n = 12$) at baseline and after vehicle (black, gray bar, $n = 12$) or indomethacin (blue, light blue bar, $n = 12$) injection. ***C***, ***D***, Mechanical and thermal sensitivity of Slurp2X KO mice before and after gabapentin treatment as compared with wild-type controls. ***C***, Latency of withdrawal from radiant heat stimuli in hindpaw plantar skin in Slurp2X wild-type mice at baseline and after vehicle (black, clear bar, $n = 10$) or gabapentin (blue, clear bar, $n = 10$) injection and Slurp2X KO mice ($n = 12$) at baseline and after vehicle (black, gray bar, $n = 10$) or gabapentin (blue, light blue bar, $n = 10$) injection. ***D***, von Frey filament 50% withdrawal threshold in hindpaw plantar skin in Slurp2X wild-type mice at baseline and after vehicle (black, clear bar, $n = 10$) or gabapentin (blue, clear bar, $n = 10$) injection and Slurp2X KO mice ($n = 12$) at baseline and after vehicle (black, gray bar, $n = 10$) or gabapentin (blue, light blue bar, $n = 10$) injection. Two-way ANOVA with Tukey's correction, $*p < 0.05$, $**p < 0.01$, $***p < 0.001$. In all panels, bar graphs show mean ± SEM, and data points represent individual female (open circles) and male (filled circles) mice backcrossed onto a C57Bl/6J background.

nonpeptidergic neurons. In immunofluorescence experiments, pad skin from Slurp2X KO mice displayed no apparent differences in IENFD compared with wild-type controls for either CGRP- or GFRα2-labeled fibers (Fig. 8*C*). However, in glabrous skin, Slurp2X KO mice exhibited an apparent reduction in IENFD for both markers, which reached statistical significance only for GFRα2-labeled fibers. These results suggest that epidermal nerve fiber density is reduced, but only in the glabrous skin of Slurp2X KO mice, and that this reduction may be differential among neuronal subtypes.

### Slurp2X KO DRG neurons display hyperactivity in vitro and in vivo

The pain hypersensitivity exhibited by Slurp2X KO mice may result from sensitized nociceptors that innervate the skin. To assess whether paw-innervating neurons were hyperexcitable in Slurp2X KO mice, we performed in vitro patch-clamp electrophysiology on DiI-labeled cultured DRG neurons. Compared with wild-type controls, Slurp2X KO DRG neurons exhibited a significant increase in the incidence of spontaneous activity as well as a reduction in rheobase among those neurons not exhibiting spontaneous activity (Fig. 9*A–D*). However, there were no differences between genotypes in RMP, membrane input resistance, AP frequency evoked by 2× rheobase, or membrane capacitance (Fig. 9*E–H*).

To circumvent confounding effects of cell dissociation and culture, we performed in vivo extracellular electrophysiological recording on the somata of DiI retrogradely labeled mouse L4 DRG neurons under deep isoflurane anesthesia (Fig. 10*A*). Fifteen wild-type neurons (2 c-fiber, 12 Aδ, and 1 Aβ) and 29

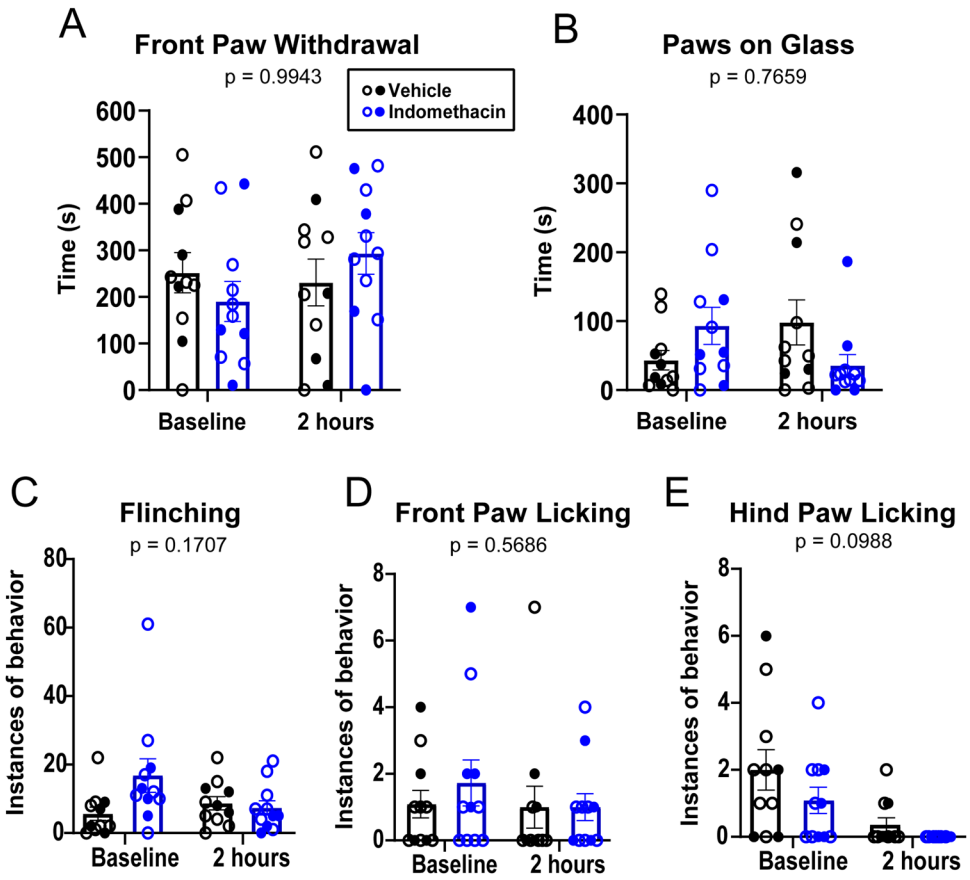


**Figure 6.** Indomethacin does not alter spontaneous pain behaviors in Slurp2X KO mice. ***A–E***, Effect of vehicle versus indomethacin intraperitoneal injection on spontaneous pain behaviors measured across 10 min in Slurp2X KO mice. ***A***, Time the animal kept a front paw withdrawn close to the body. ***B***, Time the animal kept both front paws flat on the glass surface. ***C***, Instances of front paw flinching behavior. ***D***, Instances of front paw licking behavior. ***E***, Instances of hindpaw licking behavior. Two-way ANOVA with Bonferroni's correction, $*p < 0.05$. In all panels, bar graphs show mean ± SEM, and data points represent individual female (open circles) and male (filled circles) mice backcrossed onto a C57Bl/6J background.

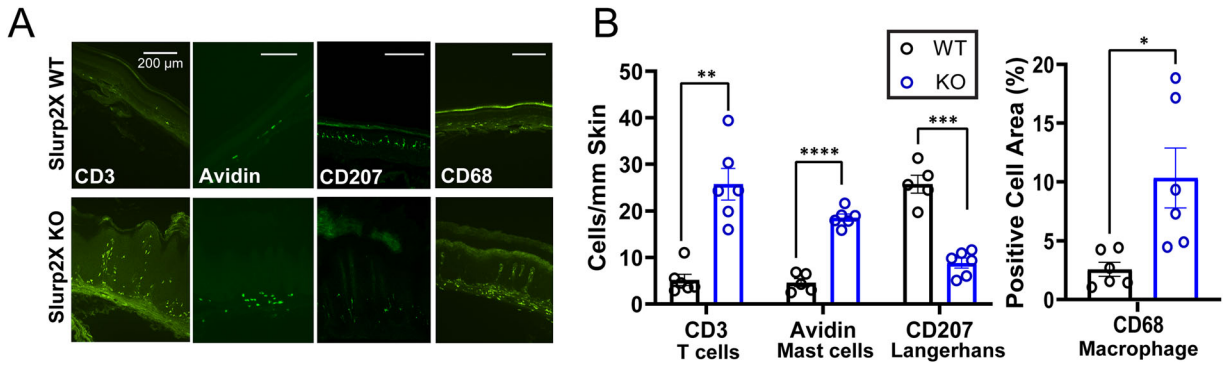


**Figure 7.** Slurp2X KO mice exhibit alterations in cutaneous immune cells and epidermal innervation. ***A***, Representative images of Slurp2X KO (KO, bottom) and wild-type (WT, top) hindpaw plantar skin immunostaining. The marker of interest is indicated in white on the wild-type image. Scale bar = 200 µm. ***B***, Quantification of immunostaining for Slurp2X KO mice (KO, blue, $n = 6$) and wild-type controls (WT, black, $n = 5–6$). Unpaired two-tailed Student's $t$ test with Welch's correction, $*p < 0.05$, $**p < 0.01$, $***p < 0.001$, $****p < 0.0001$. In all panels, bar graphs show mean ± SEM, data points represent individual mice, and mice of both sexes were used (females backcrossed onto a C57Bl/6J background for CD207 and Avidin and males on a mixed C57/Bl6/SVE-129 background for CD3 and CD68).

Slurp2X KO neurons (4 c-fiber, 25 Aδ) were included for analysis. Twenty-four percent of the Slurp2X KO neurons displayed spontaneous activity, whereas none of the recorded neurons in wild-type mice were spontaneously active (Fig. 10*B*,*C*). Given that peripheral sensitization can represent a key cause of mechanical hyperalgesia, we next asked whether the observed mechanical hyperalgesia in Slurp2X KO mice was attributable to mechanical hypersensitivity of DRG neurons. Mechanical stimuli of 2 s duration were applied to the plantar surface of the paw, since PPK is uniformly present across this surface in Slurp2X KO mice, and traces of neuronal responsiveness were recorded (Fig. 10*D*). Since the majority of the neurons assayed showed Aδ CVs, we excluded c-fibers and the single Aβ fiber from the following analysis. For Aδ neurons, the mean number

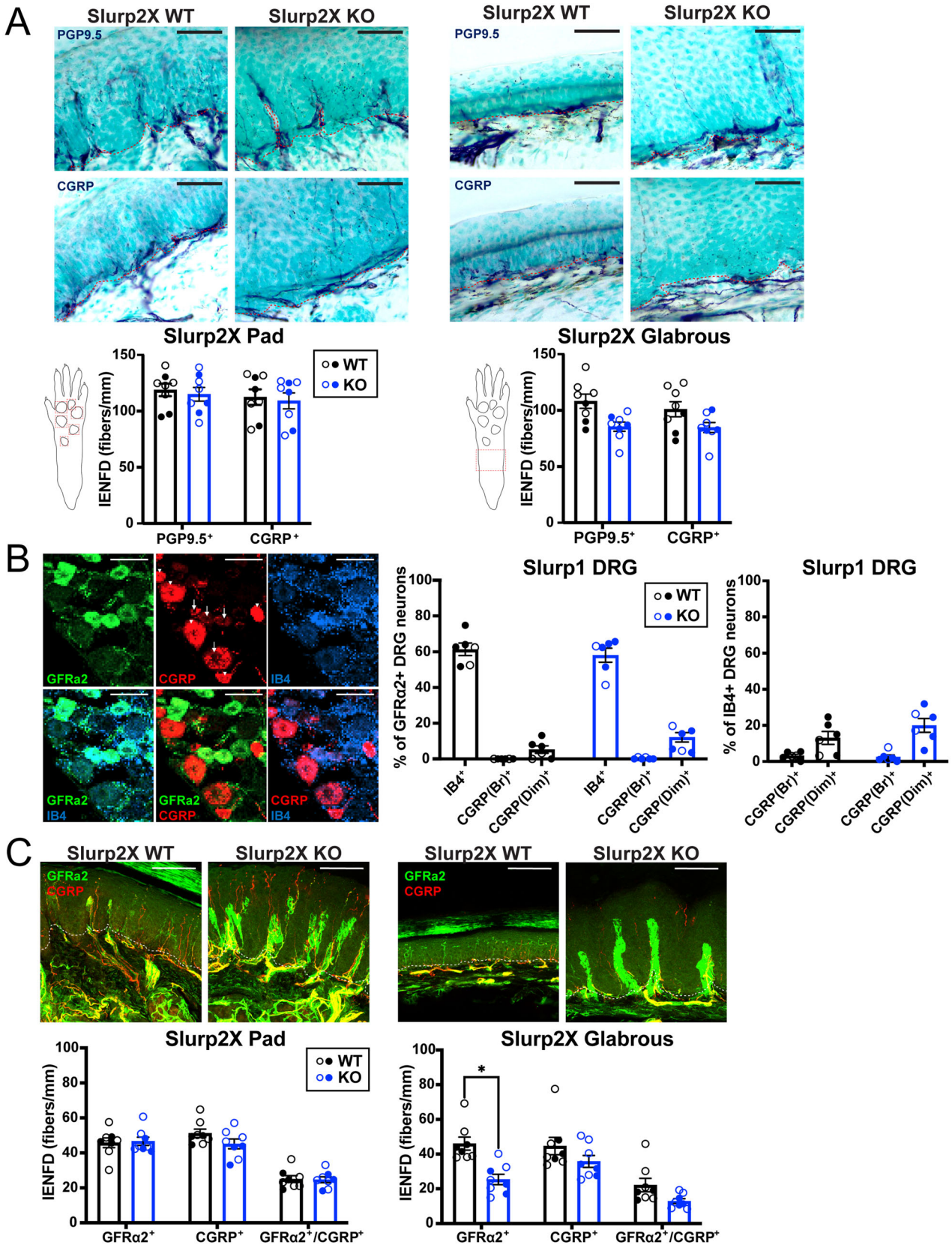


**Figure 8.** Comparison of IENFD between Slurp2X KO and wild-type mice. ***A***, Representative images of Slurp2X KO (KO, blue, $n = 8$) and wild-type control (WT, black, $n = 8$) hindpaw plantar skin immunostaining for PGP9.5 (top) and CGRP (bottom) using histochemical detection with diaminobenzidine. Scale bar = 250 µm. Red line, dermal–epidermal boundary. Unpaired two-tailed Student's *t* test with Welch's correction. ***B***, Representative images of Slurp1 KO (KO, blue, $n = 6$) and wild-type control (WT, black, $n = 6$) lumbar DRG immunostaining for GFRα2, CGRP, and IB4. White arrowheads, brightly stained CGRP-positive cell bodies. White arrows, dim or sparsely stained CGRP-positive cell bodies. The left panel shows the percentage of GFRα2 positive cells with

of APs elicited by each force was significantly greater in the Slurp2X KO mice as compared with wild-type controls (Fig. 10*E*). No significant difference in CV of Aδ fibers was observed between the Slurp2X KO and wild-type mice (Fig. 10*F*). In addition, we observed the presence of mechanically evoked afterdischarge in one neuron in a Slurp2X KO mouse whereas no such phenomenon was observed in wild-type mice. Collectively, both in vitro and in vivo electrophysiology experiments indicate that the excitability and mechanical sensitivity of paw-innervating DRG neurons are enhanced in Slurp2X KO mice, both in the mouse and when isolated from the skin environment.

## Discussion

Case reports of some individuals with MdM have described pain, anecdotally attributed to skin fractures or secondary microbial infections. However, characterization of this pain has been limited. In some other hereditary PPKs, in contrast, pain is prevalent and impactful. For example, palmoplantar pain is extremely common in individuals with PC, a condition caused by mutations in certain keratins (Eliason et al., 2012). This pain is characterized by mechanical hypersensitivity of lesioned skin areas and can be exacerbated by activities such as walking (Brill et al., 2018). Palmoplantar pain is also prevalent in OS. In some OS patients, palmoplantar pain in the context of early-life erythromelalgia may precede development of overt PPK (Duchatelet et al., 2014a,b). Case studies have reported that reversal of PPK with anti-EGFR therapy in OS patients reduces their pain (Greco et al., 2020). However, broadly efficacious therapies for pain in patients with PPK have remained elusive. Animal models of PPK showing pain hypersensitivity might therefore aid in dissecting the mechanisms underlying such pain and developing targeted analgesic therapies.

Here, we found that Slurp2X KO and Slurp1 KO mice, two genetic models of human MdM with highly penetrant PPK, exhibited hypersensitivity to mechanical and thermal stimulation of palmoplantar skin. In addition, Slurp2X KO mice exhibited increased responses to intraplantar capsaicin injection, consistent with multimodal pain hypersensitivity. In a limited number of cases, the mechanical hypersensitivity of Slurp2X KO mice, when compared with the wild type, did not reach statistical significance, likely owing to variations in experimental conditions. Many patients with painful PPK use NSAIDs to manage their pain (Milstone et al., 2005; Wallis et al., 2016), with suboptimal efficacy (Tariq et al., 2016). Treatment of Slurp2X KO mice with indomethacin, diminished thermal hyperalgesia, but mechanical sensitivity remained unchanged. This could reflect different mechanisms underlying thermal and mechanical hypersensitivity and might explain the inadequacy of NSAIDs to adequately treat pain in human PPKs. Gabapentin, which is often used to treat neuropathic pain, has also been explored as an analgesic in patients with painful PPK (Tariq et al., 2016; Smith et al., 2017). However, despite a potential neuropathic component in the Slurp2X KO mice, gabapentin failed to alleviate their thermal hypersensitivity or elevate their mechanical withdrawal thresholds.

The apparently normal heat sensitivity in the tail skin of Slurp2X knock-out mice suggests that their paw skin sensory phenotype is driven by PPK. However, a previous study reported Slurp1 expression in rat DRG neurons (Moriwaki et al., 2009), and we observed evidence of moderate expression of Slurp2 mRNA and trace expression of Slurp1 mRNA in wild-type DRG, leaving open the formal possibility that some of the phenotype of these animals is sensory neuron intrinsic. Cell type-specific Slurp knock-out will be needed to address this possibility.

Slurp2X KO and Slurp1 KO mice also exhibited increased spontaneous pain-associated behaviors, such as paw licking, flinching, and withdrawal, as compared with wild-type controls. Additionally, Slurp2X KO showed a decrease in time spent with front paws placed flat on the glass. These behaviors suggest that Slurp2X KO and Slurp1 KO mice are in a tonic state of discomfort, even in the absence of exogenous stimulation. This is consistent with findings of our electrophysiology experiments where we observed spontaneous firing as well as hyperexcitability in Slurp2X KO neurons both in vivo and in vitro. This hyperexcitability indicates that DRG neurons of Slurp2X KO mice are fundamentally changed from wild type, as these changes persist when the neurons are removed from the cutaneous environment. A caveat of these findings is that the relative uptake of DiI among sensory neuron populations may have been affected by the PPK induced alterations in skin architecture. However, the comparable CVs between the neurons compared in in vivo recordings and the comparable RMPs and capacitances among neurons compared in vitro suggest this may not be an issue. The lack of difference in RMP further suggests that the excitability changes observed are likely not attributable to changes in passive membrane excitability but may instead reflect alterations in active mechanisms, such as those involving mechanically and/or voltage-gated ion channels. The increase in spontaneous nocifensive behaviors in Slurp2X KO and Slurp1 KO mice might have impacted our evoked pain behavior analyses, in that flinching or withdrawals in knock-out mice during stimulus application could have resulted from spontaneous nociceptor firing. Reciprocally, mechanical stimulation by contact with the glass surface might contribute to "spontaneous" behaviors.

Previous studies have reported that K16 knock-out mice, a model of PC, exhibit reduced motility in an open field (Lessard and Coulombe, 2012). While no direct sensory testing has been reported in those mice, it was inferred that their reduced motility might be indicative of ongoing discomfort. Mouse genetic models of OS have failed to exhibit PPK but did show alopecia and an increased predilection toward dermatitis, with associated scratching behavior (Asakawa et al., 2006; Yoshioka et al., 2009; Yamamoto-Kasai et al., 2012). It will therefore be of value to examine both evoked and spontaneous pain behaviors in additional mouse models of PPK.

Slurp2X KO mice also show a slight decrease in epidermal nerve fiber density in hindpaw glabrous skin (but not pad skin) that was significant for nonpeptidergic GFRα2-labeled fibers but exhibited only a trend for peptidergic CGRP-labeled fibers. The timecourse of these alterations over the life of the mice (and during development of PPK) and possible alterations in

←

IB4 and CGRP staining. The right panel shows the percentage of IB4-positive cells with CGRP staining. Mann–Whitney nonparametric test. Scale bar = 50 µm. ***C***, Representative images of Slurp2X KO (KO, blue, $n = 8$) and wild-type control (WT, black, $n = 8$) hindpaw plantar skin immunostaining for GFRα2 and CGRP. Images represent max projection of *z*-stacks of equal thickness across samples. Scale bar = 100 µm. White dotted line, dermal–epidermal boundary. Mann–Whitney nonparametric test, $*p < 0.05$. In all panels, bar graphs show mean ± SEM, and data points represent individual female (open circles) and male (filled circles) mice backcrossed onto a C57Bl/6J background.

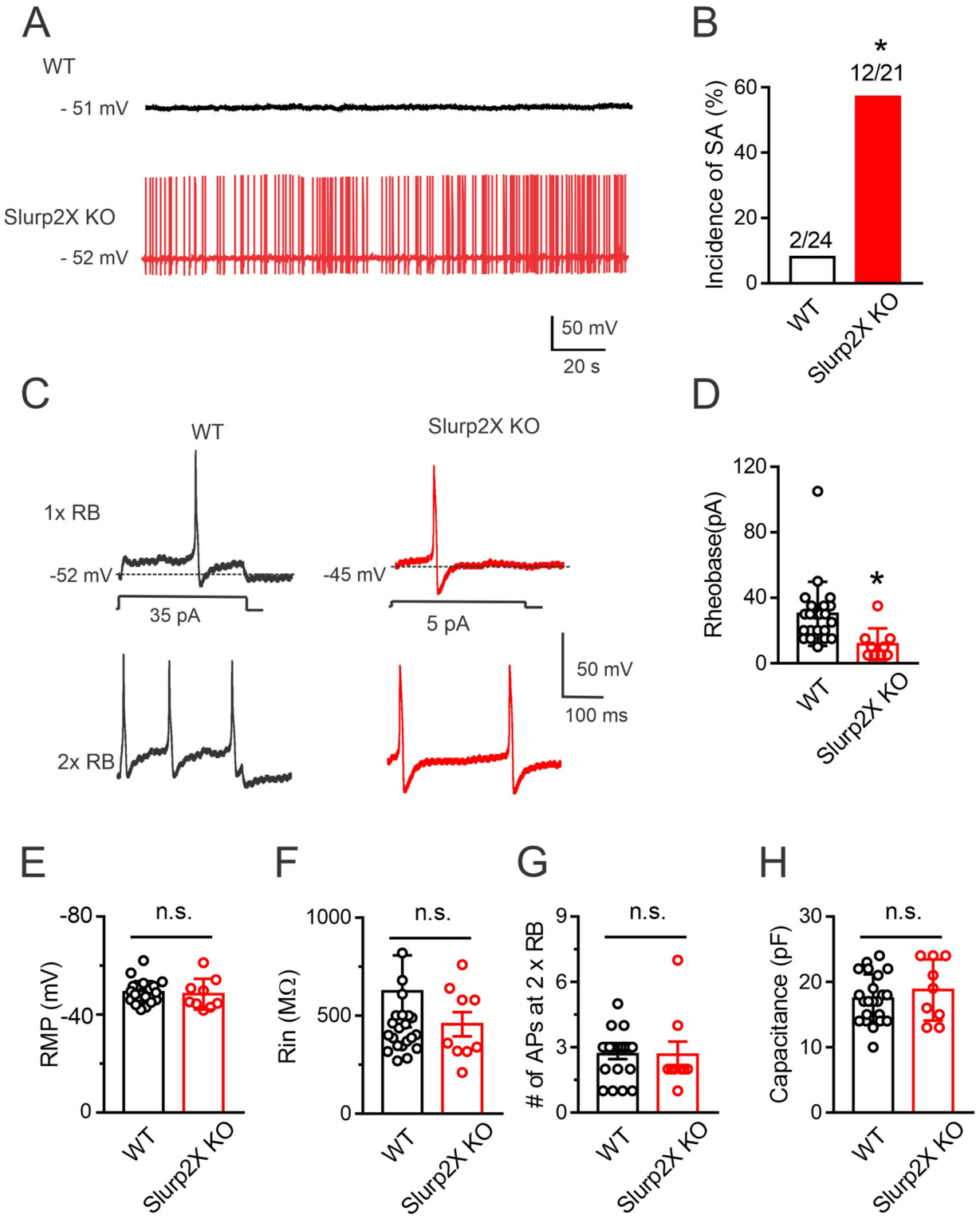


**Figure 9.** Slurp2X KO DRG neurons display hyperactivity in vitro. ***A***, Representative traces of spontaneous activity (SA) in DiI-labeled cutaneous DRG neurons of wild-type (WT, black) and Slurp2X KO (KO, red) mice. ***B***, Summary of the incidence of SA ($\chi^2$ test, $*p < 0.05$). Numbers of neurons tested are noted above graphs. ***C***, Representative traces of APs elicited at rheobase (RB) and twice RB in DiI-labeled DRG neurons that innervated glabrous skin of hindpaws of wild-type and Slurp2X KO mice. ***D–H***, Comparison of RB (***D***), RMP (***E***), input resistance (Rin, ***F***), number of APs evoked by a 2× RB current injection (***G***), and cell capacitance (***H***) in cutaneous DRG neurons between wild-type ($n = 22$ neurons from 6 mice) and Slurp2X KO mice ($n = 9$ neurons from 6 mice). Unpaired Student's $t$ test, $*p < 0.05$. Symbols represent individual neurons from mice on a mixed SVE-129 and C57/Bl6 background.

additional neuronal subtypes remain to be assessed and might provide insight into the pain phenotype of Slurp-deficient mice. A loss of epidermal innervation is reminiscent of human PC, where a trend toward reduction in IENFD, a reduction in sweat gland innervation, and altered nerve fiber morphology were observed (Pan et al., 2016). Reduced IENFD is a hallmark of many neuropathic pain disorders (Polydefkis et al., 2004; Mellgren et al., 2013). Indeed, individuals with PC sometimes

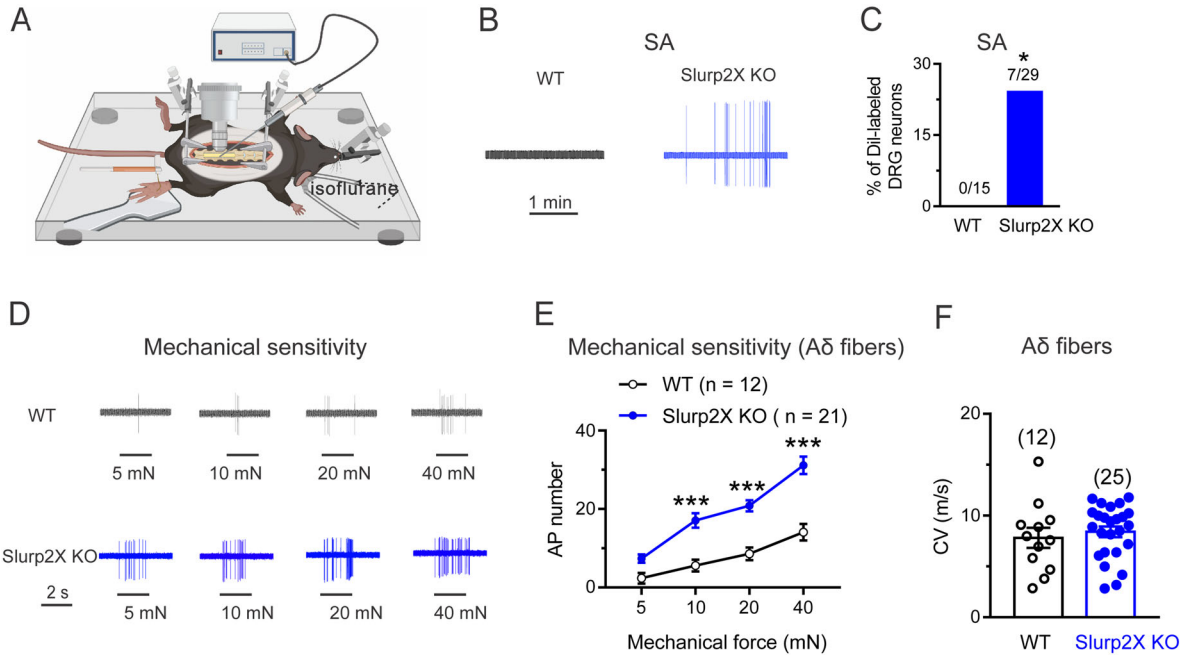


**Figure 10.** Slurp2X KO DRG neurons display hyperactivity in vivo. ***A***, Schematic of in vivo DRG extracellular recordings in anesthetized mice, generated using BioRender. ***B***, Representative traces of abnormal spontaneous activity (SA) recorded from DiI-labeled cutaneous DRG neurons that innervated glabrous skin of adult wild-type (WT, black) and global Slurp2X KO (KO, blue) mice. ***C***, Incidence of SA in wild-type and Slurp2X KO mice ($\chi^2$ test, $^*p < 0.05$). Number of neurons tested is noted above graphs. ***D***, Representative responses of cutaneous DRG neurons to mechanical stimulation (2 s in duration) of their RF with von Frey filaments (100 µm tip diameter) at the indicated bending forces in wild-type and Slurp2$^{-/-}$ mice. ***E***, The mean ± SEM number of APs evoked by each mechanical force was greater in cutaneous DRG neurons from Slurp2X KO mice ($n = 21$ neurons from 6 mice) compared with those in wild-type mice ($n = 12$ neurons from 5 mice; two-way ANOVA with Bonferroni's correction, $^{***}p < 0.001$). ***F***, Mean ± SEM conduction velocity in cutaneous DRG neurons from Slurp2X KO mice ($n = 25$ neurons from 6 mice) compared those in wild type mice ($n = 12$ neurons from 5 mice). Unpaired two-tailed Student's $t$ test, $p = 0.5621$. Symbols are from individual neurons, from mice of both sexes on a mixed SVE-129 and C57/Bl6 background.

describe their pain as sharp, throbbing, shooting, or stabbing, descriptors traditionally associated with neuropathic pain (Brill et al., 2018). A neuropathic component to pain in PC is further supported by psychophysical testing, which has revealed concurrent thermal hyposensitivity (Brill et al., 2018). While the reduced IENFD observed in Slurp2X KO mice might also be indicative of a neuropathic component, gabapentin failed to alleviate their hypersensitivity, as described above.

Our data also reveal alterations in multiple immune cell types in hindpaw glabrous skin of Slurp2X KO mice with well-established PPK. There have been reports of patients with MdM presenting with perivascular lymphocytic infiltrates and high levels of TNFα expression in the epidermis of affected skin (Kudo et al., 2020). SLURP1 has been shown to regulate macrophages and T-cell function through TNFα inhibition (Chimienti et al., 2003; Saftic et al., 2006; Tjiu et al., 2011). Interestingly, in the initial characterization of Slurp2X KO mice, H&E analysis revealed no obvious immune cell upregulation, nor was there an increase in skin proinflammatory cytokines assayed by qPCR (Allan et al., 2016). This difference between studies might be attributable to varying housing conditions between institutions or to the methods by which these cells were assessed. As with IENFD, we also have not explored the possibility of temporal variability in the immune cell response, relative to the development of the PPK. The increase in macrophages, T-cells, and avidin-binding presumptive mast cells that we observed in Slurp2X KO mice might enhance pain through an increase in cytokines and proinflammatory molecules that sensitize and/or directly activate nociceptive neurons. K16 knock-out mice also show a mixed inflammatory phenotype in affected PPK skin (Lessard et al., 2013). An increase in immune cells across models of PPK could point to a shared inflammatory pain mechanism among the disorders. The apparent reduction in Langerhans cells (LCs) in Slurp2X KO skin is also intriguing. K16 knock-out animals show an increase in epidermal LC density (Lessard et al., 2013). LC reduction is seen in patients with type 2 diabetes (Strom et al., 2014) and a variable expression pattern of LCs contributes to the pathology and severity of skin diseases like psoriasis and atopic dermatitis (Rajesh et al., 2019). LCs also regulate mast cell activation by maintaining MrgprD-expressing nonpeptidergic neurons (Zhang et al., 2021). It is therefore possible that the slight reduction in epidermal GFRα2-staining nonpeptidergic neuron density that we observed in the glabrous skin of Slurp2X KO mice is attributable to this LC deficiency and that this link between the immune system and the nervous system could be a contributing factor to PPK pain. Further studies will be required to address these possibilities.

Collectively, these data indicate that Slurp2X KO and Slurp1 KO mice exhibit a robust pain phenotype with associated electrophysiological and immunological alterations. The apparent discrepancy between these mouse models and human MdM suggests that the former may not fully recapitulate features of the latter. However, our findings suggest a broader utility of these mouse models to study mechanisms underlying PPK pain that could identify targets for the development of improved therapeutic strategies to treat such pain.

## References

Adeyo O, et al. (2014) Palmoplantar keratoderma along with neuromuscular and metabolic phenotypes in Slurp1-deficient mice. J Invest Dermatol 134:1589–1598.

Allan CM, et al. (2016) Palmoplantar keratoderma in Slurp2-deficient mice. J Invest Dermatol 136:436–443.

Allan CM, Heizer PJ, Jung CJ, Tu Y, Tran D, Young LC, Fong LG, de Jong PJ, Beigneux AP, Young SG (2018) Palmoplantar keratoderma in Slurp1/Slurp2 double-knock-out mice. J Dermatol Sci 89:85–87.

Arredondo J, Chernyavsky AI, Webber RJ, Grando SA (2005) Biological effects of SLURP-1 on human keratinocytes. J Invest Dermatol 125:1236–1241.

Asakawa M, et al. (2006) Association of a mutation in TRPV3 with defective hair growth in rodents. J Invest Dermatol 126:2664–2672.

Bennett DL, Michael GJ, Ramachandran N, Munson JB, Averill S, Yan Q, McMahon SB, Priestley JV (1998) A distinct subgroup of small DRG cells express GDNF receptor components and GDNF is protective for these neurons after nerve injury. J Neurosci 18:3059–3072.

Brill S, Sprecher E, Smith FJD, Geva N, Gruener H, Nahman-Averbuch H, Defrin R (2018) Chronic pain in pachyonychia congenita: evidence for neuropathic origin. Br J Dermatol 179:154–162.

Chaplan SR, Bach FW, Pogrel JW, Chung JM, Yaksh TL (1994) Quantitative assessment of tactile allodynia in the rat paw. J Neurosci Methods 53:55–63.

Charfeddine C, Mokni M, Kassar S, Zribi H, Bouchlaka C, Boubaker S, Rebai A, Ben Osman A, Abdelhak S (2006) Further evidence of the clinical and genetic heterogeneity of recessive transgressive PPK in the Mediterranean region. J Hum Genet 51:841–845.

Chimienti F, Hogg RC, Plantard L, Lehmann C, Brakch N, Fischer J, Huber M, Bertrand D, Hohl D (2003) Identification of SLURP-1 as an epidermal neuromodulator explains the clinical phenotype of Mal de Meleda. Hum Mol Genet 12:3017–3024.

Danso-Abeam D, et al. (2013) Olmsted syndrome: exploration of the immunological phenotype. Orphanet J Rare Dis 8:79.

Duchatelet S, Guibbal L, de Veer S, Fraitag S, Nitschke P, Zarhrate M, Bodemer C, Hovnanian A (2014a) Olmsted syndrome with erythromelalgia caused by recessive transient receptor potential vanilloid 3 mutations. Br J Dermatol 171:675–678.

Duchatelet S, Pruvost S, de Veer S, Fraitag S, Nitschke P, Bole-Feysot C, Bodemer C, Hovnanian A (2014b) A new TRPV3 missense mutation in a patient with Olmsted syndrome and erythromelalgia. JAMA Dermatol 150:303–306.

Eliason MJ, Leachman SA, Feng BJ, Schwartz ME, Hansen CD (2012) A review of the clinical phenotype of 254 patients with genetically confirmed pachyonychia congenita. J Am Acad Dermatol 67:680–686.

Favre B, Plantard L, Aeschbach L, Brakch N, Christen-Zaech S, de Viragh PA, Sergeant A, Huber M, Hohl D (2007) SLURP1 is a late marker of epidermal differentiation and is absent in Mal de Meleda. J Invest Dermatol 127:301–308.

Greco C, Leclerc-Mercier S, Chaumon S, Doz F, Hadj-Rabia S, Molina T, Boucheix C, Bodemer C (2020) Use of epidermal growth factor receptor inhibitor erlotinib to treat palmoplantar keratoderma in patients with Olmsted syndrome caused by TRPV3 mutations. JAMA Dermatol 156:191–195.

Green DP, Limjunyawong N, Gour N, Pundir P, Dong X (2019) A mast-cell-specific receptor mediates neurogenic inflammation and pain. Neuron 101:412–420.e3.

Has C, Technau-Hafsi K (2016) Palmoplantar keratodermas: clinical and genetic aspects. J Dtsch Dermatol Ges 14:123–139.

Jeon SM, Pradeep A, Chang D, McDonough L, Chen Y, Latremoliere A, Crawford LK, Caterina MJ (2024) Skin reinnervation by collateral sprouting following spared nerve injury in mice. J Neurosci 44:e1494232024.

Kalyan V, Suvvari TK, Kandula VDK, Shanker A, Matiashova L (2021) A case of Mal de Meleda: the rare presentation of palmoplantar keratoderma disease. Cureus 13:e18061.

Kudo M, et al. (2020) Abnormal keratinization and cutaneous inflammation in Mal de Meleda. J Dermatol 47:554–558.

Lauria G, Cornblath DR, Johansson O, McArthur JC, Mellgren SI, Nolano M, Rosenberg N, Sommer C, European Federation of Neurological Societies (2005) EFNS guidelines on the use of skin biopsy in the diagnosis of peripheral neuropathy. Eur J Neurol 12:747–758.

Lessard JC, Coulombe PA (2012) Keratin 16-null mice develop palmoplantar keratoderma, a hallmark feature of pachyonychia congenita and related disorders. J Invest Dermatol 132:1384–1391.

Lessard JC, Pina-Paz S, Rotty JD, Hickerson RP, Kaspar RL, Balmain A, Coulombe PA (2013) Keratin 16 regulates innate immunity in response to epidermal barrier breach. Proc Natl Acad Sci U S A 110:19537–19542.

Lindfors PH, Voikar V, Rossi J, Airaksinen MS (2006) Deficient nonpeptidergic epidermis innervation and reduced inflammatory pain in glial cell line-derived neurotrophic factor family receptor alpha2 knock-out mice. J Neurosci 26:1953–1960.

Mellgren SI, Nolano M, Sommer C (2013) The cutaneous nerve biopsy: technical aspects, indications, and contribution. Handb Clin Neurol 115:171–188.

Milstone LM, Fleckman P, Leachman SA, Leigh IM, Paller AS, van Steensel MA, Swartling C (2005) Treatment of pachyonychia congenita. J Investig Dermatol Symp Proc 10:18–20.

Morais e Silva FA, Cunha TV, Boeno Edos S, Steiner D (2011) Mal de Meleda: a report of two cases of familial occurrence. An Bras Dermatol 86:S100–S103.

Moriwaki Y, Watanabe Y, Shinagawa T, Kai M, Miyazawa M, Okuda T, Kawashima K, Yabashi A, Waguri S, Misawa H (2009) Primary sensory neuronal expression of SLURP-1, an endogenous nicotinic acetylcholine receptor ligand. Neurosci Res 64:403–412.

Pan B, Byrnes K, Schwartz M, Hansen CD, Campbell CM, Krupiczojc M, Caterina MJ, Polydefkis M (2016) Peripheral neuropathic changes in pachyonychia congenita. Pain 157:2843–2853.

Perez C, Khachemoune A (2016) Mal de Meleda: a focused review. Am J Clin Dermatol 17:63–70.

Pinho-Ribeiro FA, Verri WA Jr, Chiu IM (2017) Nociceptor sensory neuron-immune interactions in pain and inflammation. Trends Immunol 38:5–19.

Polydefkis M, Hauer P, Sheth S, Sirdofsky M, Griffin JW, McArthur JC (2004) The time course of epidermal nerve fibre regeneration: studies in normal controls and in people with diabetes, with and without neuropathy. Brain 127:1606–1615.

Qu L, Caterina MJ (2016) Enhanced excitability and suppression of a-type K(+) currents in joint sensory neurons in a murine model of antigen-induced arthritis. Sci Rep 6:28899.

Qu L, Li Y, Pan X, Zhang P, LaMotte RH, Ma C (2012) Transient receptor potential canonical 3 (TRPC3) is required for IgG immune complex-induced excitation of the rat dorsal root ganglion neurons. J Neurosci 32:9554–9562.

Qu L, Zhang P, LaMotte RH, Ma C (2011) Neuronal Fc-gamma receptor I mediated excitatory effects of IgG immune complex on rat dorsal root ganglion neurons. Brain Behav Immun 25:1399–1407.

Rajesh A, Wise L, Hibma M (2019) The role of Langerhans cells in pathologies of the skin. Immunol Cell Biol 97:700–713.

Saftić V, Rudan D, Zgaga L (2006) Mendelian diseases and conditions in Croatian island populations: historic records and new insights. Croat Med J 47:543–552.

Sakiyama T, Kubo A (2016) Hereditary palmoplantar keratoderma "clinical and genetic differential diagnosis". J Dermatol 43:264–274.

Schiller S, Seebode C, Hennies HC, Giehl K, Emmert S (2014) Palmoplantar keratoderma (PPK): acquired and genetic causes of a not so rare disease. J Dtsch Dermatol Ges 12:781–788.

Schindelin J, et al. (2012) Fiji: an open-source platform for biological-image analysis. Nat Methods 9:676–682.

Schuttenhelm BN, Duraku LS, Dijkstra JF, Walbeehm ET, Holstege JC (2015) Differential changes in the peptidergic and the non-peptidergic skin innervation in rat models for inflammation, dry skin itch, and dermatitis. J Invest Dermatol 135:2049–2057.

Smith FJD, Hansen CD, Hull PR, Kaspar RL, McLean WHI, O'Toole E, Sprecher E (2017) Pachyonychia congenita. In: *Gene reviews* (Adam MP, Feldman J, Mirzaa GM, et al. eds), Seattle, WA: University of Washington.

Strom A, Bruggemann J, Ziegler I, Jeruschke K, Weiss J, Al-Hasani H, Roden M, Ziegler D, Group GDS (2014) Pronounced reduction of cutaneous Langerhans cell density in recently diagnosed type 2 diabetes. Diabetes 63:1148–1153.

Tariq S, Schmitz ML, Kanjia MK (2016) Chronic foot pain due to pachyonychia congenita in a pediatric patient: a successful management strategy. A A Case Rep 6:305–307.

Tejada J, Chaim K, Morato S (2018) X-PloRat: a software for scoring animal behavior in enclosed spaces. Psicol Teor Pesqui 33.

Tjiu JW, Lin PJ, Wu WH, Cheng YP, Chiu HC, Thong HY, Chiang BL, Yang WS, Jee SH (2011) SLURP1 mutation-impaired T-cell activation in a family with Mal de Meleda. Br J Dermatol 164:47–53.

Totsch SK, Sorge RE (2017) Immune system involvement in specific pain conditions. Mol Pain 13:1744806917724559.
Wajid M, Kurban M, Shimomura Y, Christiano AM (2009) Mutations in the SLURP-1 gene underlie Mal de Meleda in three Pakistani families. J Dermatol Sci 56:27–32.
Wallis T, Poole CD, Hoggart B (2016) Can skin disease cause neuropathic pain? A study in pachyonychia congenita. Clin Exp Dermatol 41:26–33.
Wang L, et al. (2019) Neuronal FcgammaRI mediates acute and chronic joint pain. J Clin Invest 129:3754–3769.
Yamamoto-Kasai E, Imura K, Yasui K, Shichijou M, Oshima I, Hirasawa T, Sakata T, Yoshioka T (2012) TRPV3 as a therapeutic target for itch. J Invest Dermatol 132:2109–2112.
Yoshioka T, Imura K, Asakawa M, Suzuki M, Oshima I, Hirasawa T, Sakata T, Horikawa T, Arimura A (2009) Impact of the Gly573Ser substitution in TRPV3 on the development of allergic and pruritic dermatitis in mice. J Invest Dermatol 129:714–722.
Zhang S, et al. (2021) Nonpeptidergic neurons suppress mast cells via glutamate to maintain skin homeostasis. Cell 184:2151–2166.e16.